



HAL
open science

Summertime surface PM 1 aerosol composition and size by source region at the Lampedusa island in the central Mediterranean Sea

Marc Mallet, Barbara d'Anna, Aurélie Mème, Maria Chiara Bove, Federico Cassola, Giandomenico Pace, Karine Desboeufs, Claudia Di Biagio, Jean-Francois Doussin, Michel Maillé, et al.

► To cite this version:

Marc Mallet, Barbara d'Anna, Aurélie Mème, Maria Chiara Bove, Federico Cassola, et al.. Summertime surface PM 1 aerosol composition and size by source region at the Lampedusa island in the central Mediterranean Sea. *Atmospheric Chemistry and Physics*, 2019, 19 (17), pp.11123-11142. 10.5194/acp-19-11123-2019 . hal-02352573

HAL Id: hal-02352573

<https://hal.science/hal-02352573>

Submitted on 6 Nov 2019

HAL is a multi-disciplinary open access archive for the deposit and dissemination of scientific research documents, whether they are published or not. The documents may come from teaching and research institutions in France or abroad, or from public or private research centers.

L'archive ouverte pluridisciplinaire **HAL**, est destinée au dépôt et à la diffusion de documents scientifiques de niveau recherche, publiés ou non, émanant des établissements d'enseignement et de recherche français ou étrangers, des laboratoires publics ou privés.



Summertime surface PM₁ aerosol composition and size by source region at the Lampedusa island in the central Mediterranean Sea

Marc D. Mallet^{1,2,3}, Barbara D'Anna^{2,4}, Aurélie Mème^{2,a}, Maria Chiara Bove^{5,6}, Federico Cassola^{5,b}, Giandomenico Pace⁷, Karine Desboeufs¹, Claudia Di Biagio¹, Jean-Francois Doussin¹, Michel Maille¹, Dario Massabò⁵, Jean Sciare⁸, Pascal Zapf¹, Alcide Giorgio di Sarra⁷, and Paola Formenti¹

¹LISA, CNRS UMR7583, Université Paris Est Créteil (UPEC), Université de Paris, Institut Pierre Simon Laplace (IPSL), Créteil, France

²IRCELYON, CNRS UMR 5652, Univ. Lyon1, Lyon, France

³Centre National d'Etudes Spatiales (CNES), Toulouse, France

⁴LCE, CNRS UMR 7376, Aix-Marseille Université, Marseille, France

⁵Department of Physics & INFN, University of Genoa, Genoa, Italy

⁶ARPAL Physical Agents and Air Pollution Sector, La Spezia, Italy

⁷Laboratory for Observations and Analyses of Earth and Climate, ENEA, Rome, Italy

⁸The Cyprus Institute, Energy, Environment and Water Research Center, Nicosia, Cyprus

^anow at: Bruker, Lyon, France

^bcurrently at: ARPAL CFMI-PC, Genoa, Italy

Correspondence: Paola Formenti (paola.formenti@lisa.u-pec.fr)

Received: 26 February 2019 – Discussion started: 12 March 2019

Revised: 3 July 2019 – Accepted: 24 July 2019 – Published: 3 September 2019

Abstract. Measurements of aerosol composition and size distributions were taken during the summer of 2013 at the remote island of Lampedusa in the southern central Mediterranean Sea. These measurements were part of the ChArMEx/ADRIMED (Chemistry and Aerosol Mediterranean Experiment/Aerosol Direct Radiative Forcing on the Mediterranean Climate) framework and took place during Special Observation Period 1a (SOP-1a) from 11 June to 5 July 2013.

From compact time-of-flight aerosol mass spectrometer (cToF-AMS) measurements in the size range below 1 μm in aerodynamic diameter (PM₁), particles were predominately comprised of ammonium and sulfate. On average, ammonium sulfate contributed 63 % to the non-refractory PM₁ mass, followed by organics (33 %). The organic aerosol was generally very highly oxidized (f_{44} values were typically between 0.25 and 0.26). The contribution of ammonium sulfate was generally higher than organic aerosol in comparison to measurements taken in the western Mediterranean but is consistent with studies undertaken in the eastern basin.

Source apportionment of organics using a statistical (positive matrix factorization) model revealed four factors: a hydrocarbon-like organic aerosol (HOA), a methanesulfonic-acid-related oxygenated organic aerosol (MSA-OOA), a more oxidized oxygenated organic aerosol (MO-OOA) and a less oxidized oxygenated organic aerosol (LO-OOA). The MO-OOA was the dominant factor for most of the campaign (53 % of the PM₁ OA mass). It was well correlated with SO_4^{2-} , highly oxidized and generally more dominant during easterly air masses originating from the eastern Mediterranean and central Europe. The LO-OOA factor had a very similar composition to the MO-OOA factor but was more prevalent during westerly winds, with air masses originating from the Atlantic Ocean, the western Mediterranean and at high altitudes over France and Spain from mistral winds. The MSA-OOA factor contributed an average 12 % to the PM₁ OA and was more dominant during the mistral winds. The HOA, representing observed primary organic aerosol, only contributed 8 % of the average PM₁ OA during the campaign.

Even though Lampedusa is one of the most remote sites in the Mediterranean, PM₁ concentrations ($10 \pm 5 \mu\text{g m}^{-3}$)

were comparable to those observed in coastal cities and sites closer to continental Europe. Cleaner conditions corresponded to higher wind speeds. Nucleation and growth of new aerosol particles was observed during periods of north-westerly winds. From a climatology analysis from 1999 to 2012, these periods were much more prevalent during the measurement campaign than during the preceding 13 years. These results support previous findings that highlight the importance of different large-scale synoptic conditions in determining the regional and local aerosol composition and oxidation and also suggest that a non-polluted surface atmosphere over the Mediterranean is rare.

1 Introduction

The Mediterranean Sea is a unique marine environment, surrounded by mountain ranges and high coastal human populations from Africa, Europe and Asia, and the two largest deserts in the world: the Sahara to the south and Arabian Desert to the east. It presents a diverse and dynamic atmospheric composition and is projected to undergo significant changes in the contribution of freshwater (Sanchez-Gomez et al., 2009), sea surface temperature and precipitation (Mariotti et al., 2015) over the coming decades. The burning of fossil fuels, including shipping pollution, in southern Europe and in large Mediterranean cities, as well as natural sources of aerosol such as sea salt, forest fires and mineral dust, provide a highly complex and dynamic mixture of organic and inorganic aerosol and aerosol precursors in this region (Lelieveld et al., 2002). Elevated aerosol loadings over the Mediterranean basin have been attributed to the long-range transport of continental anthropogenic aerosols (Perrone et al., 2013; Sciare et al., 2003, 2008) and mineral dust transported from Africa (Querol et al., 2009b; Koçak et al., 2007). Boundary layer observations in the eastern Mediterranean have shown a significant influence of long-range-transported continental pollution from southern and central Europe (Sciare et al., 2003). Furthermore, biomass burning aerosol has frequently been observed over the basin, in particular during the dry season in summer when forest fires are more common (Bougiatioti et al., 2014; Minguillon et al., 2015; Pace et al., 2005). Long-range plumes from North American fires have also been observed at high altitudes (Formenti et al., 2002; Ortiz-Amezcuca et al., 2014; Brocchi et al., 2018; Ancellet et al., 2016).

Previous long-term observations of the chemical composition of aerosol in the Mediterranean have shown that PM₁₀ (particulate mass with aerodynamic diameter less than 10 µm) is composed of secondary ammonium sulfate, primary and secondary organic aerosol from fossil fuels or biogenic origins, with contributions from natural aerosols from the Sahara and sea spray (Bove et al., 2016; Koulouri et al., 2008; Schembari et al., 2014; Calzolari et al., 2015). Mineral

and sea salt contributions are significantly lower in PM_{2.5} particle fraction (Querol et al., 2009a). Coarse-mode particles contribute to the direct radiative effect over the Mediterranean (Perrone and Bergamo, 2011; Meloni et al., 2006) and can also act as condensation sinks for pollutants (Pikridas et al., 2012). Smaller (submicron) aerosol particles, while also contributing efficiently to the total aerosol optical depth in this region (Formenti et al., 2018), can also act as efficient cloud condensation nuclei and therefore have an influence on cloud formation, lifetime and precipitation (Haywood and Boucher, 2000). Understanding the impact of different natural and anthropogenic sources on the regional composition of the atmosphere is therefore important in our understanding of the influences they have on the climate over the Mediterranean basin and surrounding regions. It is also now widely recognized that aerosols contribute to adverse health effects in humans (World Health Organization, 2016).

Consideration of both the local and regional meteorology is needed to characterize the sources and ageing of aerosols (Petit et al., 2017). The National Oceanic and Atmospheric Administration (NOAA)'s Hybrid Single-Particle Lagrangian Integrated Trajectory model (HYSPLIT; Stein et al., 2015) and other trajectory models (e.g. FLEXPART; Stohl et al., 2005) have become widely used resources in atmospheric studies to compute the backward or forward trajectories of air masses at any point on Earth. They can be useful for identifying the possible origin of a particular episode associated with elevated concentrations of aerosols or gases. Combined with in situ measurements over longer time periods, they provide a more holistic approach in understanding the link between local or region meteorology and atmospheric composition (Schmale et al., 2013; Tadros et al., 2018; Zhou et al., 2016). This is particularly useful for remote sites where local emissions are insignificant or infrequent.

Investigation of the aerosol physical and chemical properties can also help distinguish their respective sources. Positive matrix factorization (PMF; Paatero, 1997; Paatero and Tapper, 1994) has proved to be a useful statistical tool in identifying aerosol sources or ageing processes of organics. The source apportionment of PM_{2.5} and PM₁₀ over the Mediterranean, from the PMF method, has been investigated in recent works and showed a large spatial variability in source contributions (Becagli et al., 2012, 2017; Calzolari et al., 2015; Amato et al., 2016; Diapouli et al., 2017). The PMF approach was also used to study the aerosol source and ageing processes by utilizing the complex nature of organic aerosol in the Mediterranean (e.g. Hildebrandt et al., 2010, 2011; Bougiatioti et al., 2014; Minguillon et al., 2016; Arndt et al., 2017; Michoud et al., 2017). This approach has become increasingly feasible, with the recent widespread implementation of instruments capable of providing real-time, high time- and mass-resolved non-refractory aerosol composition, such as aerosol mass spectrometers (Ulbrich et al., 2009). PMF models have shown to successfully resolve the

bulk composition of submicron organic aerosol into the contributions from various primary sources (e.g. biomass burning, fossil fuel burning, cooking aerosol) but can also reveal the contributions and characteristics of secondary organic aerosol (SOA) (Zhang et al., 2011). Factors with similar mass spectra are consistently observed, albeit with different contributions at measuring sites all around the world. The most commonly observed primary organic aerosol factors are hydrocarbon-like OA (HOA), usually from fossil fuel burning as well as biomass burning (BBOA), while SOA can be usually separated into at least two factors, with low-volatility oxygenated OA (LV-OOA) and semi-volatile OOA (SV-OOA) as common examples (Zhang et al., 2011; Crippa et al., 2014). Other types of OOA have also been observed, such as marine-OOA (Schmale et al., 2013), although these are more difficult to resolve given the shift towards more uniform OA composition with ageing.

The Chemistry-Aerosol Mediterranean Experiment (ChArMEx) collaborative research programme, and the Aerosol Direct Radiative Impact on the regional climate in the MEDiterranean region (ADRI-MED) project within, were undertaken to investigate the chemistry and climate interactions within the Mediterranean (Mallet et al., 2016). From 11 June to 5 July 2013, numerous experimental setups were deployed across the western and central Mediterranean in what is called “Special Observation Period – 1a” (SOP-1a), including intensive airborne measurements (Denjean et al., 2016). Two supersites were set up at Ersá (at the northern tip of Corsica island, France) and at the Lampedusa island (Italy), approximately 1000 km apart on a north-to-south axis in order to characterize surface aerosol chemical, physical and optical properties (Mallet et al., 2016). Numerous secondary sites established along the Mediterranean coasts in Spain, Italy and Corsica beyond SOP-1a have also provided valuable knowledge of the atmospheric composition in the western and central Mediterranean regions (Chrit et al., 2017, 2018; Becagli et al., 2017).

In this paper, we present the first detailed characterization of PM₁ in the central remote Mediterranean region, using measurements of size-resolved chemical composition on the island site of Lampedusa during ChArMEx/ADRI-MED SOP-1a. We investigate the source apportionment of PM₁ by considering their chemical and microphysical properties along with ancillary PM₁₀, gaseous and meteorological data, air-mass back trajectories as well as complementary data collected at the Ersá site in Corsica.

2 Experimental

2.1 Sampling sites

Observations took place at the Roberto Sarao station on the island of Lampedusa (35°31'5" N, 12°37'51" E; 20 m a.s.l.) from 11 June to 5 July 2013. Ancillary measurements for



Figure 1. The Mediterranean basin. The two sites considered in this study, Lampedusa and Ersá, are indicated in white dots. Image is courtesy of © Google Earth 2019.

this study taken at Ersá at the northern tip of Cap Corse (42°58'5" N, 9°22'49" E; 560 m a.s.l.) are also considered. The positions of the stations are shown in Fig. 1.

2.2 Instrumentation, measurements and data

Instruments at the Lampedusa supersite were housed in the PEGASUS (Portable Gas Field and Aerosol Sampling Unit) station, a portable observatory initiated by LISA, described in Mallet et al. (2016). Relevant to this study, a cToF-AMS (Aerodyne Inc., Billerica, USA) was used to measure the size-resolved composition of non-refractory particulate matter below 1 µm (NF-PM₁) (Drewnick et al., 2005). Data were collected with a 3 min time resolution. The cToF-AMS was operated from a certified total suspended particulate (TSP) sampling head (Rupperecht and Patashnick, Albany, NY, USA), followed by a cyclone impactor cutting off aerosol particles larger than 1 µm in aerodynamic diameter (using a flow rate of 16 lpm). A Nafion drier was used; however, the relative humidity at the inlet of the cToF-AMS was checked throughout the campaign and was always below 55 %.

A particle-into-liquid sampler (Metrohm PILS; Orsini et al., 2003) was installed on a TSP inlet and collected samples approximately every hour. Denuders to remove acid/base gases were not used. Samples were analysed for major inorganic and organic anions (F⁻, Cl⁻, NO₃⁻, SO₄²⁻, PO₄³⁻, HCOO⁻, CH₃COO⁻, (COO⁻)₂) and cations (Na⁺, NH₄⁺, K⁺, Ca²⁺, Mg²⁺) using ion chromatography (Metrohm, model 850 Professional IC) equipped with Metrosep A Supp 7 pre-column and column for anions measurements and Metrosep C4-250 mm pre-column and column for cation measurements and a 500 µL injection loop. The device was operated with a 1 h time resolution.

A 13-stage rotating cascade impactor (NanoMOUDI model 125B; Marple et al., 1991) was used to measure the size-segregated inorganic elemental composition. The NanoMOUDI impactor, also operated from the TSP inlet, al-

lows the separation of the particles into 13 size classes from 10 nm to 10 μm diameters with a backup stage. Each sample was collected for 3 d with a flow rate of 10 lpm to ensure enough material was collected on each impactor stage. The 47 mm diameter polytetrafluoroethylene filters (2 μm pore size) were used and coated with high-quality vacuum grease (Dekati DS-515) to avoid bouncing. They were then analysed using X-ray fluorescence (PW-2404 spectrometer by PANalytical™) for the particulate elemental concentrations for elements from Na to Pb as described in Denjean et al. (2016).

A scanning mobility particle sizer (SMPS) measured the mobility number size distribution of aerosols every 3 min from 14.6 to 661.2 nm diameter. The instrument is composed by an X-ray electrostatic classifier (TSI Inc., model 3080) and a differential mobility analyser (DMA; TSI Inc., model 3081) and a condensation particle counter (CPC; TSI Inc., model 3775) operated at 1.5/0.3 L min⁻¹ aerosol/sheath flows. Data were corrected to take into account the particle electrical charging probabilities, the CPC counting efficiency and diffusion losses. Each scan was recorded with a 5 min time resolution. A drier was not used on the SMPS inlet, and therefore the size distributions reported are for ambient conditions.

A GRIMM optical particle counter (OPC; GRIMM Inc., model 1.109) was used to measure the number size distribution over 31 size classes ranging from 0.26 up to 32 μm (nominal diameter range assuming the aerosol refractive index of latex spheres in the calibration protocol). The instrument was operated at a 6 s resolution and data were acquired as 3 min averages.

The equivalent black carbon mass concentration (eBC) was determined by the measurement of light attenuation at 880 nm performed by a spectral aethalometer (Magee Sci. model AE31) operated at a 2 min time resolution and equipped with a TSP particle inlet. As the evaluation of eBC is used as a qualitative tracer of pollution, the factory mass conversion factor of 16.6 m² g⁻¹ was applied to the raw measurement of attenuation without further corrections.

The meteorological measurements (air pressure, temperature, relative humidity, wind direction and speed and precipitation) were collected by a Vaisala Milos 500 station with a sampling rate of 10 min. The wind sensor was installed on a 10 m meteorological tower, while the air temperature and humidity were measured at a height of 2 m.

2.3 Data analysis

2.3.1 Analysis of the cToF-AMS data

The cToF-AMS data set was processed using two different software analysis tools. The first makes use of the widely used and standard Igor Pro package, Squirrel (version 1.57G). This software processes the raw data and analyses the unit-mass resolution (UMR) output with a fragmenta-

tion table reported in Aiken et al. (2008). The second method uses a cumulative peak-fitting analysis and residual analysis and allows the separation of multiple isobaric peaks not taken into account in the traditional analysis of unit mass resolution Squirrel data treatment (Muller et al., 2011). Uncertainties in the major chemical species from the cToF-AMS are typically of the order of ±20 % (Drewnick et al., 2005).

The ionization efficiency (IE) with respect to nitrate anions was calculated every 5–6 d using nebulized 350 nm mobility diameter ammonium nitrate particles (values varied between 1.42 × 10⁻⁷ and 1.53 × 10⁻⁷). The relative IE (RIE) of ammonium was slightly higher than the default value and was 4.3 based on the mass spectrum of ammonium nitrate data from IE calibrations. The RIE of sulfate was determined by comparing the theoretical and the measured concentration of a solution of ammonium nitrate and ammonium sulfate and was determined to be the default value of 1.2. For the organic fraction, the default value of 1.4 was used. For each of the major species, a composition-dependent collection efficiency was applied as proposed by Middlebrook et al. (2012) and was on average 0.549, very similar to the default value of 0.55.

The PM₁ sea salt concentration was estimated in the cToF-AMS by applying a scaling factor of 102 to the ion fragment (using the cumulative peak-fitting analysis described in Muller et al., 2011) at 57.98 assigned to NaCl as proposed by Ovadnevaite et al. (2012). This scaling factor was determined by nebulizing monodisperse 300 nm (mobility diameter) NaCl particles into the cToF-AMS and comparing the NaCl⁺ signal to the total mass calculated using the number concentration from a CPC-3010. This calibration was done after the campaign but with similar tuning conditions. The sea salt SO₄²⁻ (ss-SO₄²⁻) was calculated as 0.252 · 0.3 · [seasalt], where 0.252 is the mass ratio of SO₄²⁻ to Na⁺ in sea salt and 0.3 is the mass ratio of Na⁺ to sea salt (Ghahremaninezhad et al., 2016). Given these assumptions, the uncertainty in the sea salt concentrations is likely to be significantly higher than the typical 20 %, although the total contribution of sea salt to the PM₁ fraction was very small (0.30 μg m⁻³; <4 %).

Unconstrained positive matrix factorization was performed on both the unit-mass resolution spectra of organic aerosol as well as the peak-fitted peaks identified as organics using PMF2 v2.08D. This method requires a matrix for both the organic signals as well as the errors associated with the organics. For the peak-fitted signals, errors for each mass were estimated as

$$\Delta I/I = \sqrt{\alpha^2 t + (\beta + 1)}, \quad (1)$$

where I is the ion signal, ΔI is the absolute uncertainty in the ion signal, α and β are constants (1.2 and 0.001, respectively), and t is the instrumental sampling time in seconds (Drewnick et al., 2009; Allan et al., 2003). For both UMR and peak-fitted inputs, up to eight factors were investigated

by altering the seeds from 0 to 50 in increments of 1 and the peaks from -1 to 1 in increments of 0.1 . This approach is explained in Ulbrich et al. (2009).

2.3.2 Air-mass back-trajectory calculation and cluster analysis

In order to determine potential source regions for aerosols measured at Lampedusa during the SOP-1a, a series of cluster analyses was performed on HYSPLIT air-mass back trajectories as per the following. Weekly GDAS1 (Global Data Assimilation System; 1° resolution) analysis trajectory files were downloaded from the Air Resources Laboratory (ARL) of the NOAA archive. The 144 h air-mass back trajectories were then calculated every hour over the measurement period with an ending point at Lampedusa (height of 45 m) using HYSPLIT (Stein et al., 2015) from within the R package, SplitR. Cluster analyses were then performed on these calculated trajectories using a trajectory clustering function within the R package, OpenAir (Carslaw and Ropkins, 2012). Clustering was done using two different methods to calculate the similarity between different trajectories. The first uses the Euclidean distance between the latitude and longitude of each trajectory point (a total of 144 in this case, representing each hour prior to the arrival at the receptor site). The second uses the similarity of the angles of each trajectory from the origin. These two methods are described in Sirois and Bottenheim (1995). For each clustering method, the number of clusters was altered from 2 up to 10. A total of six clusters identified using the Euclidean-distance method were selected, producing a realistic separation of the air-mass back trajectories and distinct and physically meaningful differences in aerosol composition and size. An additional clustering analysis was also performed over 3 and 6 h intervals and using 96 h back trajectories and yielded similar results.

3 Results and discussion

3.1 Analysis of local and synoptic meteorology

The analysis of the hourly resolved 144 h air-mass back trajectories provides an indication of the origin of the air masses sampled at Lampedusa during the field campaign. Six distinct clusters are identified (Fig. 2). Cluster 1 (eastern Mediterranean) is representative of air masses that circulate around the eastern–central Mediterranean basin before arriving at the Lampedusa site (average altitude of 400 m). Cluster 2 (central Europe) is representative of air masses arriving from central Europe (average altitude of 800 m). Cluster 3 (Atlantic) is representative of more marine-like air masses that predominately originate over the Atlantic Ocean, pass over the Strait of Gibraltar between Spain and Morocco, and cross the western Mediterranean basin (average altitude of 500 m). Cluster 4, western Europe, cluster 5, mistral (low), and cluster 6, mistral (high), all have similar angular trajec-

tories but are distinguishable by their different wind speeds and altitudes (although the Euclidian method of cluster analysis only considers differences in horizontal distances). The two mistral clusters typically originate over the northern Atlantic Ocean, travel over France at a high altitude before descending over the western Mediterranean and travelling with relatively higher wind speeds towards Lampedusa. The altitude of mistral (high) was, on average, higher than mistral (low) (1400 and 1000 m, respectively) and also coincided with higher wind speeds at Lampedusa (13 and 9 m s^{-1} , respectively). In comparison, the trajectories of the western Europe cluster spent much more time circulating at lower altitudes (700 m, on average) over the western Mediterranean basin and, to a certain extent, east of the Lampedusa site.

As a complement, the pressure, temperature, relative humidity, wind speed and direction time series recorded at the station are shown in Fig. 3. Two main weather regimes are observed: the former characterized by intense (up to nearly 20 m s^{-1}) north-westerly winds, persisting for several days (10–13 and 22–30 June) and cool temperatures, whereas the latter associated with low-gradient anticyclonic conditions and light winds from the east or south-east, also favouring warmer temperatures (14–21 June and 1–3 July). Temperatures were relatively stable over the sampling period, fluctuating between approximately 18.5 and 28.2°C . The relative humidity typically ranged between 70 % and 82 % with very few and very brief episodes of drier air masses (relative humidity close to or below 50 %). The wind speed and direction distributions during the campaign can be compared to the June–July climatology from 1999 to 2012 (Fig. 4). During the sampling period of this study, the frequency of winds from the north-westerly sectors was nearly double the average when compared to normal conditions, approaching 40 % with high winds speeds exceeding 10 m s^{-1} observed during more than 20 % of the time.

Data of sea level pressure and 1000 mbar meridional wind component composite anomalies obtained from the National Centers for Environmental Prediction (NCEP)/National Center for Atmospheric Research (NCAR) reanalysis (Kalnay et al., 1996) indicate that this particular situation was induced by a dipolar pattern, characterized by positive pressure anomalies in the western Mediterranean and negative ones in the eastern part of the basin (see Fig. S1 in the Supplement). This produced a persisting, stronger-than-normal gradient over southern Italy. As a consequence, surface dust episodes typically driven by strong south or south-easterly winds, associated to cyclonic systems moving along northern African coasts, were basically absent during the campaign.

3.2 Aerosol composition

The dry NR-PM₁ concentrations measured at Lampedusa by the cToF-AMS ranged from 1.9 to $33.4\text{ }\mu\text{g m}^{-3}$, with a mean of $10.2\text{ }\mu\text{g m}^{-3}$ over the sampling period. Sulfate contributed the most to the measured NR-PM₁ mass ($41\% \pm 9\%$ on av-

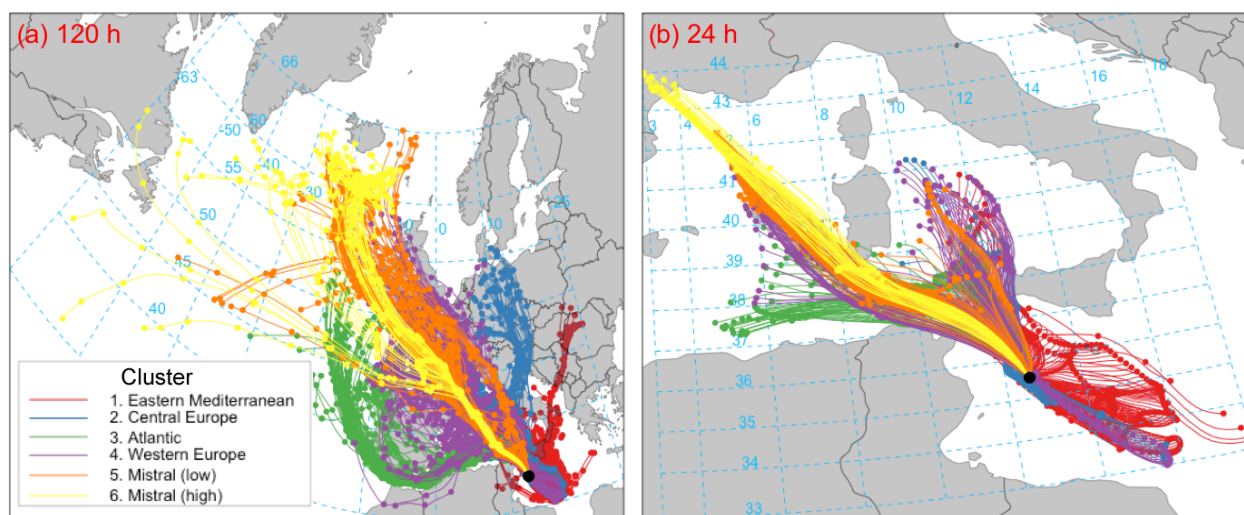


Figure 2. (a) Hourly 144 h (6 d) back trajectories from Lampedusa from 10 June to 5 July 2013, cut off at 120 h (5 d). Colours represent the assigned cluster. (b) The same as panel (a) but cut off at 24 h.

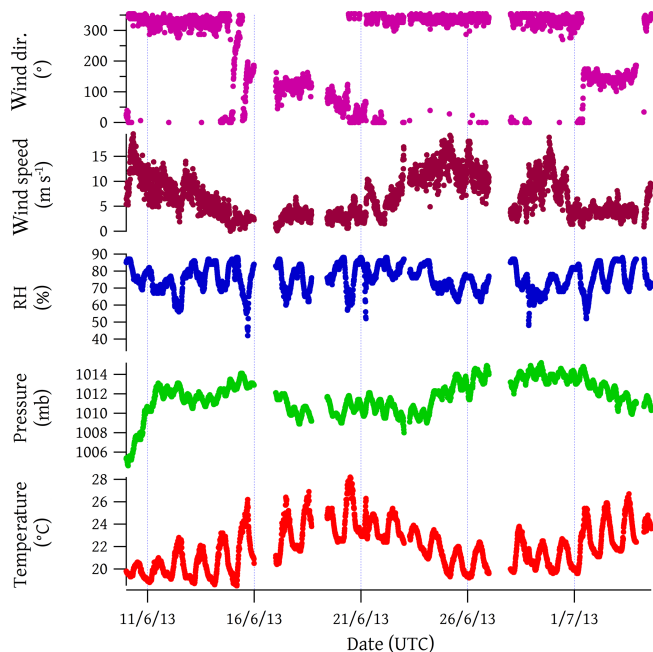


Figure 3. Meteorological conditions (wind direction and speed, relative humidity, pressure and temperature) measured at the Lampedusa site during SOP-1a.

erage), followed by significant contributions from organics ($31\% \pm 8\%$) and ammonium ($17\% \pm 3\%$). The eBC, nitrate and sea salt (scaled from the NaCl component of m/z 58) contributed 6% ($\pm 4\%$), 1% ($\pm 0.4\%$) and 3% ($\pm 2\%$), respectively. Figure 5 shows the total PM₁ concentration (calculated as the sum of the individually measured species), with contribution from each of the species, as well as the calculated PM₁ mass concentration from the SMPS (assum-

ing an average density based on the composition data). There was reasonable agreement (slope of 0.62; $R^2 = 0.67$) between the PM₁ mass concentration calculated from composition measurements and the SMPS, with discrepancy observed during periods of high sulfate concentrations from the eastern Mediterranean. This could be due to a combination of a broader accumulation mode exceeding the upper size limits of the cToF-AMS inlet, differences in sampling line relative humidity or unaccounted-for variations in the collection efficiency. This figure also contains an indication of the air-mass origin over the sampling period.

During most of the campaign there was reasonable agreement (slope of 1; $R^2 = 0.6$) between the PM₁ SO₄²⁻ (cToF-AMS) and the TSP SO₄²⁻ (PILS) concentration, with the exception of periods of high sea salt concentrations when the TSP SO₄²⁻ were significantly higher (slope of 0.5; $R^2 = 0.2$ for TSP Cl concentrations $> 10 \mu\text{g m}^{-3}$; see Fig. S2). Supporting measurements of the size-segregated composition from the cascade impactor corroborate this, indicating a higher contribution of elemental sulfur in the coarse mode during periods of higher sea salt (Fig. S3). These periods corresponded to the mistral air masses, characterized by higher wind speeds and indicated the role of coarse sea salt particles in acting as a condensation sink for sulfate species. If these events are frequent, this could have important implications for the radiative properties of these aerosols by altering the scattering properties and potentially cloud condensation nuclei concentrations and composition.

Figure 6 shows the organic mass, split according to different OA factors from the PMF of the OA peaks. From the unconstrained PMF of the UMR and peak-fitted organic mass spectra, the most meaningful solution was found from a four-factor solution of the UMR analysis (see Figs. S4 and S5 for the mass reconstruction and time series' residuals). This has

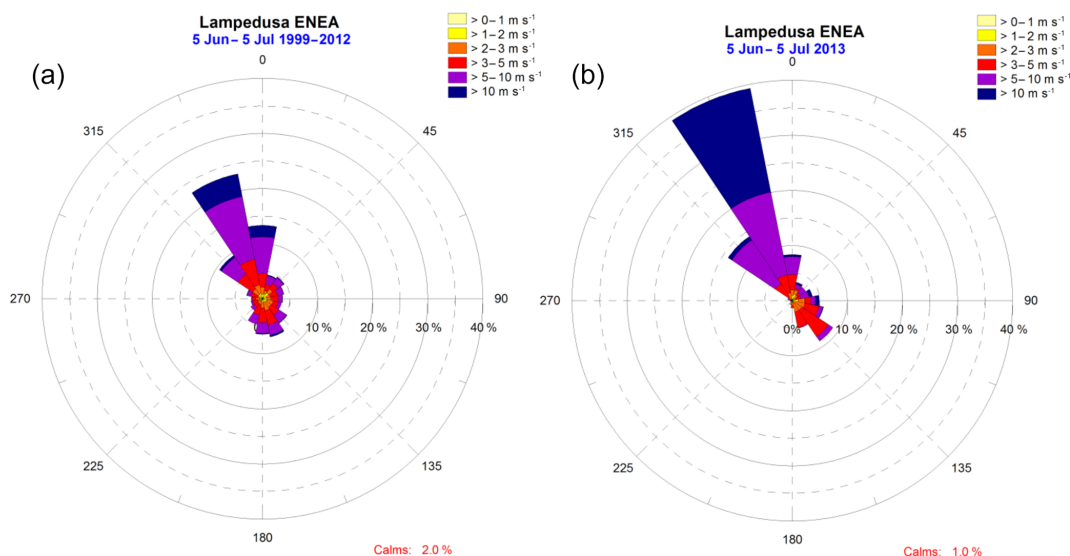


Figure 4. Wind speed and direction at Lampedusa during the period from 5 June to 5 July during the years 1999–2012 (a) and during this campaign (b).

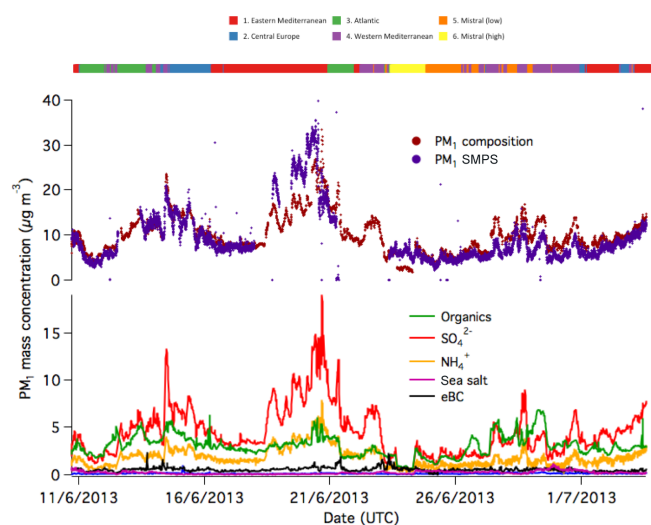


Figure 5. The time series of PM₁ mass concentration, coloured by the relative contribution from each species. The top bar is coloured according to the air-mass origin.

resulted in one factor resembling a primary organic aerosol and three oxygenated organic aerosol (OOA) factors. Herein, we label these factors HOA (hydrocarbon-like OA), MO-OOA (more oxidized OOA), LO-OOA (less oxidized OOA) and MSA-OOA (methanesulfonic-acid-related OOA).

These factors were compared with ambient organic mass spectra listed in the AMS Spectral Database (Ulbrich et al., 2009). The spectra for the OOA factors (see Fig. 7) were strongly correlated with each other ($R > 0.97$) and all three were similar to a continental OOA factor observed in a ship campaign in the Arctic (Chang et al., 2011), as well as a low-

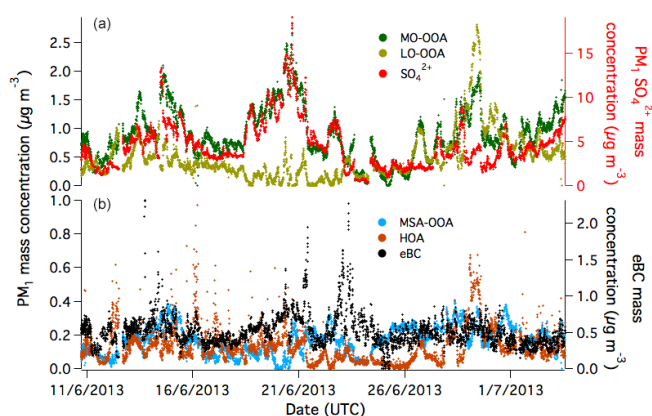


Figure 6. The time series of the PM₁ more oxidized OOA (MO-OOA), less oxidized (LO-OOA) and sulfate (a) and methanesulfonic-acid-related OOA (MSA-OOA), hydrocarbon-like OA (HOA) and eBC (b).

volatility OOA factor identified in Paris (Crippa et al., 2013). Despite the similarities in their mass spectra, they exhibited different diurnal trends (Fig. 7) and time series that were associated with different wind directions and air masses and were therefore not recombined into a single OOA factor.

The MO-OOA factor was the most dominant factor during the field campaign ($\sim 53\%$ of the total OA mass) and was typical of low-volatility/highly oxidized OOA observed in many other studies, in the Mediterranean, with high contributions of m/z 44 ($f_{44} = 0.31$) (e.g. Hildebrandt et al., 2010, 2011). This factor was the most prominent during air masses from the eastern Mediterranean, central Europe and Atlantic (contributing to 71 %, 58 % and 55 % to OA, respectively) and was strongly correlated with ammonium sulfate

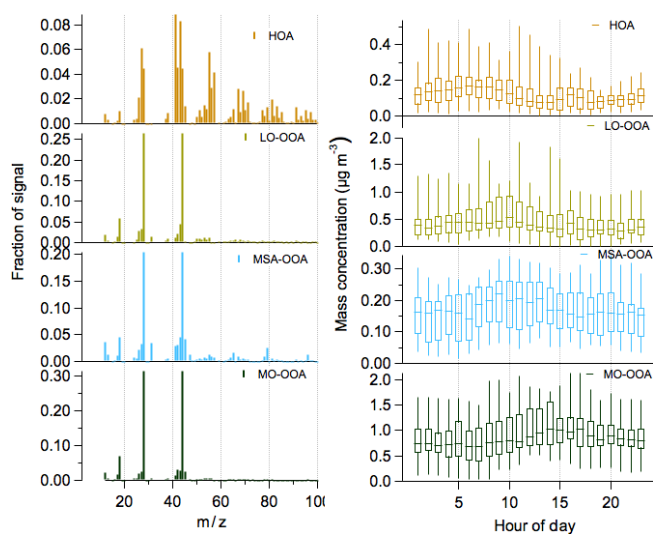


Figure 7. The mass spectra for the four PMF factors (HOA: hydrocarbon-like organic aerosol, LO-OOA: less oxidized OOA, MO-OOA: more oxidized OOA, MSA-OOA: methanesulfonic-acid-related OOA) retrieved from the PMF analysis of unit-mass resolution data.

($R^2 = 0.68$) over the whole campaign. It also had a distinct diurnal trend, with concentrations increasing during daylight hours, indicative of photochemical processing. The LO-OOA factor was slightly less oxygenated ($f_{44} = 0.26$) and exhibited a different time series ($R^2 = 0.04$), related to different air masses, than the MO-OOA. The less oxygenated OOA factor has also been associated with semi-volatile species and is often labelled as SV-OOA (Jimenez et al., 2009). Despite a distinct diurnal profile similar to previously reported SV-OOA factors (with a peak in the early morning), we refrain from labelling our LO-OOA this way because the mass spectrum was generally much more oxygenated and contained less f_{43} than typically reported SV-OOA (see Fig. 9).

The MSA-OOA factor contributed approximately 12 % of the total OA during the campaign and is likely related to the biogenic emission and processing of dimethyl sulfide (DMS) from phytoplankton in the Mediterranean. This factor was also highly oxygenated ($f_{44} = 0.20$) but contains key peaks related to the fragmentation of MSA from the electron impact of the cToF-AMS. The most prominent of these peaks were m/z 96 (CH_4SO_3^+), 79 (CH_3SO_2^+), 78 (CH_2SO_2^+), 65 (HSO_2^+) and 45 (CH_3^+). A similar factor was observed at Bird Island in the south Atlantic Ocean (Schmale et al., 2013), albeit without the contribution of significant m/z 44, suggesting a more aged or mixed aerosol during this campaign. A distinct diurnal pattern for the MSA-OOA was not observed.

While the MO-OOA, LO-OOA and MSA-OOA factors represent secondary organic aerosol and were the most dominant contribution of OA during the campaign (92 % on average), a primary organic aerosol factor was observed and

identified here as HOA. The mass spectrum of the HOA factor was characteristic of spectra observed in other studies, with prominent peaks at m/z 95, 91, 83, 81, 71, 69, 57, 55, 43 and 41. Although HOA is typically associated with emissions from incomplete combustion (Zhang et al., 2005), it was not well correlated with other expected tracers such as eBC, CO and NO_x . This HOA was typically associated with south-westerly winds of low speed ($<5 \text{ m s}^{-1}$; see Fig. 10) and peaked at approximately 06:00 LT each morning. The poor correlation between the HOA factor and eBC could have been due to a variety of local sources with different HOA and eBC emission factors, a mixing of the PMF factor with some small peaks not associated with combustion processes or from regional HOA that has undergone some transport without significant oxidation. The signal fraction of each m/z of the mass spectrum of the HOA factor however had strong correlations ($0.69 < R < 0.89$) with numerous HOA factors from other studies (Hersey et al., 2011; Ulbrich et al., 2009; Ng et al., 2011; Lanz et al., 2007; Zhang et al., 2005).

3.3 Comparison with other observations around the Mediterranean

There are many factors that could influence the composition, the concentration and oxidation level of different aerosol species over the Mediterranean. These include different aerosol sources which can follow different seasonal or yearly trends (e.g. biogenic emissions) as well as the existing aerosol load and the meteorological conditions that drive transport, dilution and ageing processes. The majority of previous studies of detailed PM₁ aerosol composition have been taken at coastal sites around the Mediterranean (Mohr et al., 2012; Minguillón et al., 2015, 2016; El Haddad et al., 2013; Bozzetti et al., 2017) which could be expected to observe higher concentrations than at Lampedusa due to proximity to sources (e.g. traffic, fossil fuel use, heating, biomass burning, industrial activities). Aside from Lampedusa and the observations presented in this study, measurements at Finokalia and Cap Corse could be considered the most remote sites where these measurements have been taken. Similar to the comparison of NR-PM₁ measurements from Europe, North America and east Asia made by Zhang et al. (2007), Fig. 8 summarizes the recent observations of NR-PM₁ composition from measurements in and around the Mediterranean basin (see Tables S1 and S2 for more details that are displayed in Fig. 8).

The PM₁ mass loading observed at Lampedusa is comparable to most of these other studies performed at both remote marine sites and coastal sites in the Mediterranean. With the exception of sites in the eastern Mediterranean, OA was the dominant NR-PM₁ constituent and summertime OA was generally considered mostly secondary, comprised of SV-OOA and LV-OOA with small contributions of HOA. For remote sites, the results are consistent with a predomi-

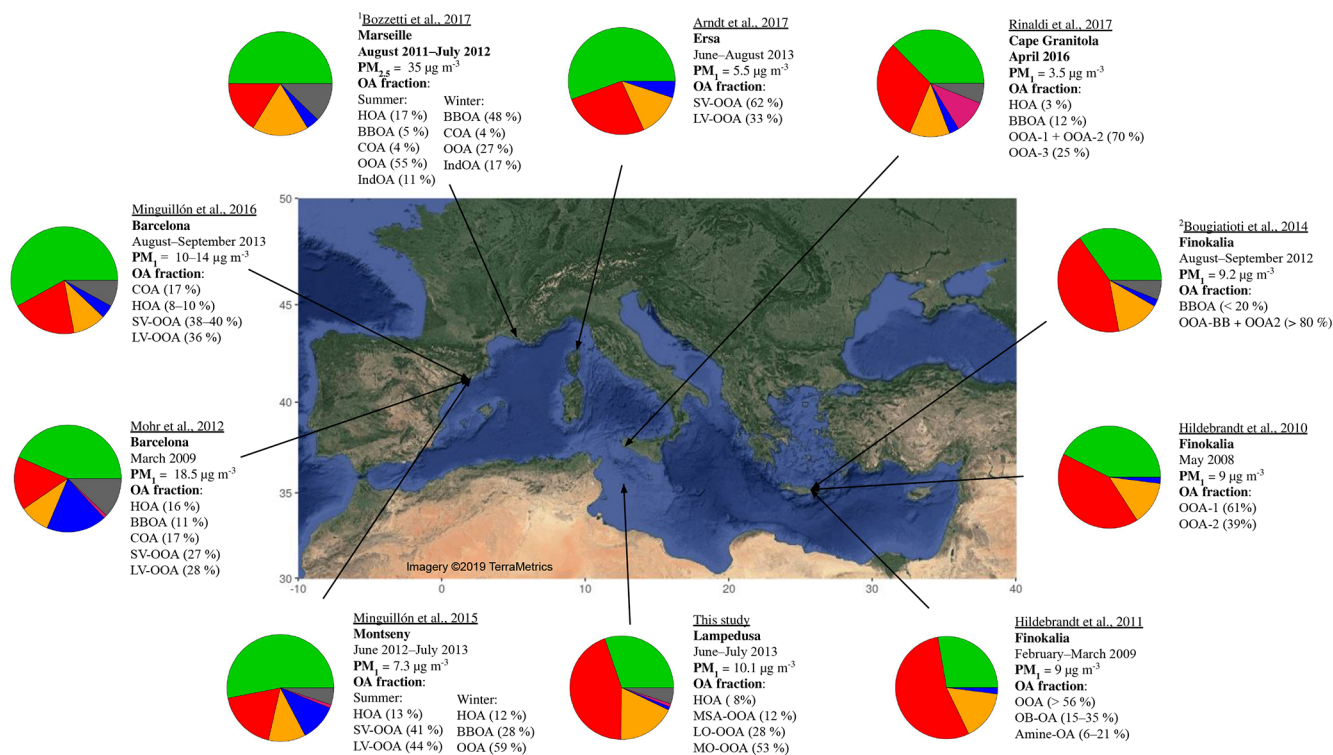


Figure 8. A summary of studies that have investigated NR-PM₁ composition (including PMF of OA) around the Mediterranean basin. Only studies that have investigated PMF-based OA source apportionment are reported. Pie charts display the average concentration during each study, where green corresponds to organics, red to sulfates, orange to ammonium, blue to nitrate, pink to either chlorides or sea salt and black to elemental or black carbon. The OA fraction acronyms correspond to the following: HOA: hydrocarbon-like organic aerosol, SV-OOA: semi-volatile oxygenated organic aerosol, LV-OOA: low-volatility oxygenated organic aerosol, BBOA: biomass burning organic aerosol, COA: cooking organic aerosol, OOA: oxygenated organic aerosol, F4: factor 4 (unidentified PMF factor), IndOA: industry-related organic aerosol, OB-OA: olive-branch organic aerosol. See Tables S1 and S2 for further details about the sampling locations, instruments used and pie chart values. ¹ This study collected on PM_{2.5} filters and nebulized into an HR-ToF-AMS. ² Excludes fire periods.

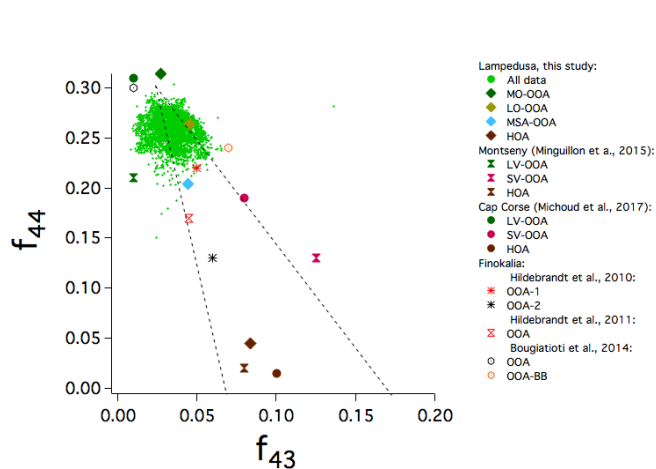


Figure 9. f_{43} (the ratio of m/z 43 to the total OA) against f_{44} (ratio of m/z 44 to the total OA). The triangle is considered to encapsulate typical atmospheric values of OA according to Ng et al. (2010). The values for the various PMF factors from this study and other studies conducted in the remote Mediterranean are also displayed.

nance of OA in PM₁ fraction in summer. PMF analysis of Q-AMS measurements at the Finokalia remote site in the eastern Mediterranean in the summer of 2008 showed two OOA factors and a distinct lack of HOA (Hildebrandt et al., 2010). A more recent study during the late 2012 summer at Finokalia observed periods influenced by biomass burning but otherwise also observed mostly oxygenated organic aerosol (Bougiatioti et al., 2014). Measurements undertaken in the western Mediterranean at Cap Corse from 11 June to 6 August 2013 encompassed the sampling period of this study. For the period from 15 July to 5 August, PMF analysis showed 55 %, 27 % and 13 % contributions of organic matter, sulfate and ammonium to non-refractory PM₁ (Michoud et al., 2017). Secondary oxygenated volatile organic compounds (VOCs) dominated the VOC spectrum during the campaign and were very well correlated with submicron organic aerosol. PMF analysis on the OA revealed a three-factor solution where SV-OOA and LV-OOA were dominant, contributing by 44 % and 53 %, respectively, with a 4 % HOA contribution. From the same measurements but reported over the extended period from 11 June to 5 August, there was

a higher LV-OOA contribution (62 %) (Arndt et al., 2017) which is in agreement with our observations of MO-OOA at Lampedusa. The OA was mostly portioned into MO-OOA and LO-OOA (81 %), indicative of well-aged or oxidized secondary organic aerosol from long-range transport of pollutants.

Figure 9 displays the behaviour of the f_{44} and f_{43} fragments obtained during the field campaign. f_{44} , a proxy for OA oxidation (Jimenez et al., 2009), is calculated as the ratio of the mass at m/z 44 (mostly CO₂⁺) to the total OA, while f_{43} , equal to the ratio of m/z 43 (mostly C₂H₃O⁺) to the total OA, typically represents less-aged OA. f_{44} was ~ 0.26 for the majority of the sampling period (Q1: 0.25; Q3: 0.27), while f_{43} was 0.036 (Q1: 0.028; Q3: 0.041). The campaign values are compared to values from the spectra for the four PMF factors and those observed in other field campaigns in the remote Mediterranean. The dotted lines (the so-called Ng triangle) encapsulate the f_{44} and f_{43} values of atmospheric OA from a vast number of studies (Ng et al., 2010), with the most aged OA in the top left corner and the most fresh in the bottom right. The high f_{44} values and the dominance of the highly oxygenated MO-OOA and LO-OOA factors show that the organic aerosol was extremely aged compared to other measurements.

3.4 Links to meteorology

The contribution of the major submicron chemical species and OA sources is further explained in the following by linking the measured and apportioned concentrations to the local meteorology (i.e. wind speed and wind direction) and to the air-mass back trajectories to account for the long-range transport of aerosol as well as more distant sources. The bivariate polar plots of these PM₁ species and f_{44} as a function of wind speed and direction are shown in Fig. 10.

Considering that the sampling site on Lampedusa is on the north-east tip of the island, it is evident that the SO₄²⁻ and NH₄⁺ were likely a result of north-easterly marine air masses, in agreement with previous results (e.g. Bove et al., 2016). Sea salt concentrations were highest during high north-westerly wind speeds. Higher concentrations of NO₃⁻, HOA and some of the periods with elevated eBC concentrations were observed during low-speed south-westerly winds, likely a result of the human settlements and activity on the island of Lampedusa (population of ~ 6000 located to the south-west of the sampling site). Besides, the polar plot for eBC showed a patchier pattern, indicative of more local or point sources, and the elevated signals were likely due to air masses passing over ship plumes. Although the mass spectra for the LO-OOA and MO-OOA factors were very similar, their bivariate polar plots indicate different sources or photochemical processes. The MO-OOA was more prominent during north-easterly winds, indicating the most aged organics were influenced by air masses from the eastern Mediterranean, either from long-range transport or from cir-

culatation of closer pollution sources, while the LO-OOA was more dominant during north-westerly wind directions and air masses from over the western Mediterranean. Figure 11 shows the average contribution of each species during different air-mass periods (see Table S2 for the mean concentrations and standard deviations).

The highest concentrations of PM₁ were observed during eastern Mediterranean and central Europe air-mass periods, when significant lifetime over the lower-altitude marine environment and/or higher SO₂ emissions allowed the conversion and condensation of sulfate. These aged aerosols are corroborated by the high number concentrations within the accumulation mode during these periods relative to other periods, measured by the SMPS as well as the size-resolved sulfate composition, as discussed in the next section. In contrast to the eastern Mediterranean and central European air masses, sulfate concentrations were relatively low during the two mistral air masses. This behaviour has been found also in PM₁₀, with elevated values of sea salt aerosol and low non-sea-salt sulfate during mistral events (Becagli et al., 2017). The organic mass concentration was relatively uniform across the periods of different air-mass origins, with the exception of the high mistral winds which yielded OA concentrations approximately half the rest of the campaign and a higher contribution of MSA-OOA in comparison with other periods. The higher contribution of MO-OOA compared with LO-OOA from eastern air masses, and vice versa during western air masses, could be indicative of different OA sources prior to oxidation or due to different photochemical ageing between the two directions.

3.5 Aerosol size distributions

There are distinctions between the measured PM₁ size distributions during periods of different air-mass origins (Fig. 12). It should be noted that these size distributions are under ambient conditions without an inlet drier which could shift the size distribution to larger sizes if water is present. The ambient relative humidity for each air-mass back-trajectory cluster was eastern Mediterranean (53 %), central Europe (61 %), Atlantic (74 %), western Mediterranean (70 %), mistral (low) (67 %) and mistral (high) (74 %). Although the higher temperature inside the PEGASUS mobile laboratory could lower the relative humidity at the sampling point of the SMPS with respect to the ambient relative humidity, this was not measured or logged during the campaign.

Consistent with the higher concentrations of sulfate and ammonium species, the eastern Mediterranean and central Europe had the most pronounced accumulation modes with respect to those from other clusters due to the presence of accumulation-mode sulfate (see Fig. S6 for the size-resolved chemical composition). In contrast, the mistral (high) air masses had very few particles in the accumulation mode and were mostly dominated by nucleation-mode (> 14 nm observations only) and Aitken-mode particles, in terms of number.

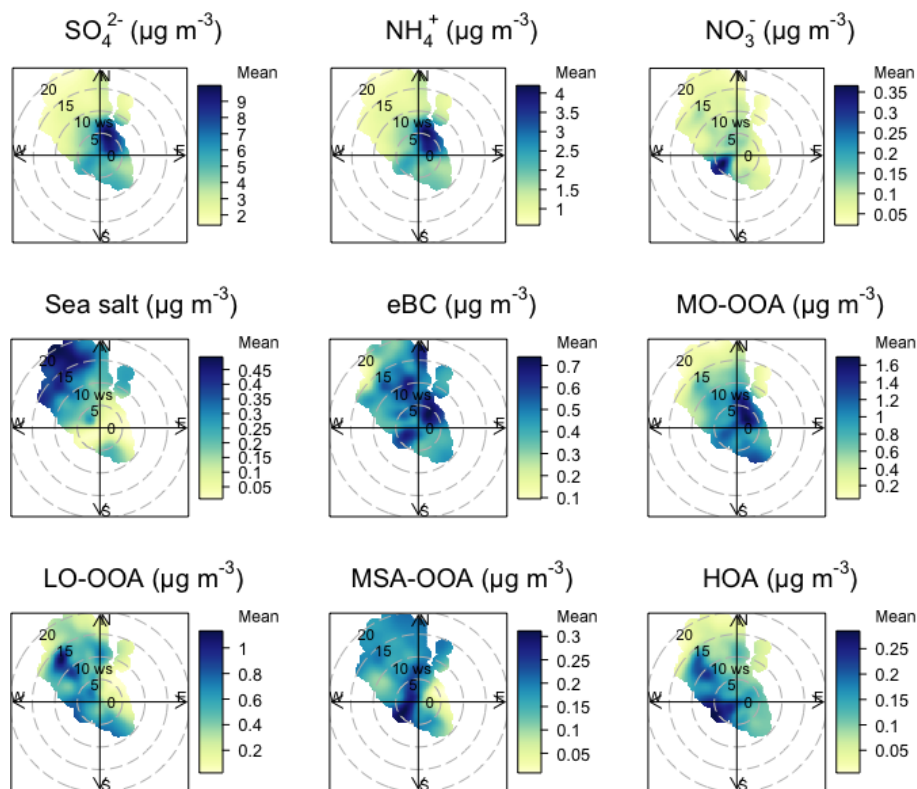


Figure 10. Bivariate polar plots of mean concentrations of PM₁ species and f_{44} at Lampedusa. The angle represents the arrival wind direction, the radius represents the wind speed, and the colours represent the mean concentrations for the respective wind directions and winds.

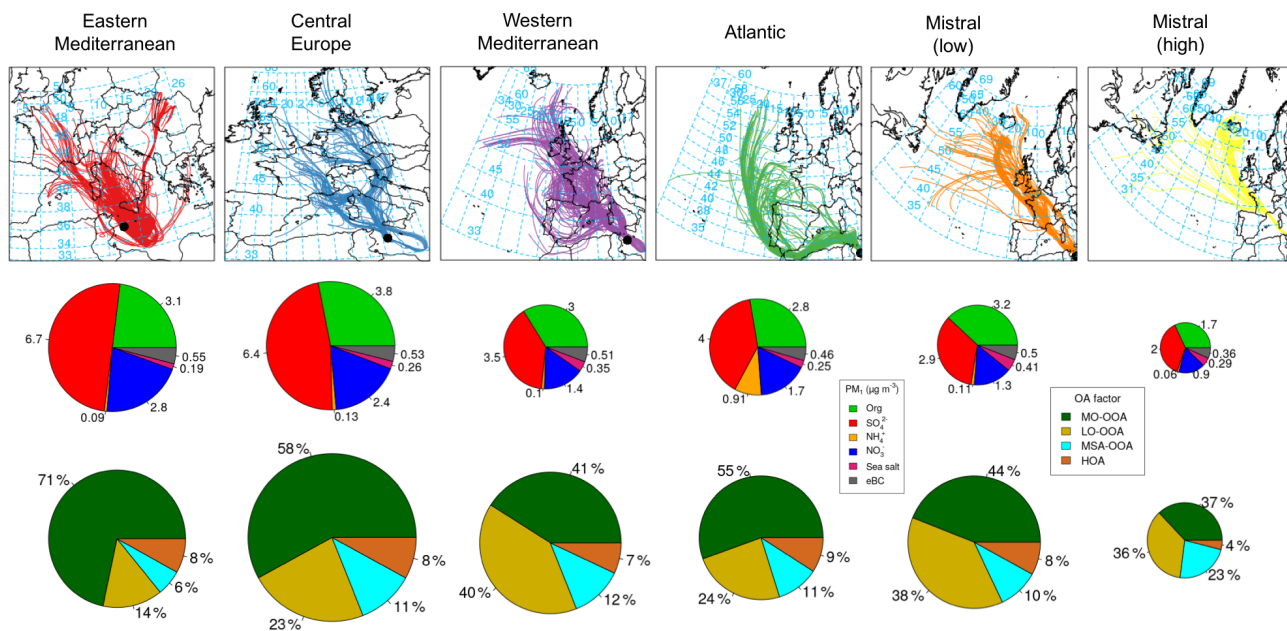


Figure 11. The 144 h air-mass back trajectories (top) assigned to each cluster; (middle) the PM₁ composition for each air-mass cluster and (bottom) the contribution of OA factors for each air-mass cluster. The diameters for the PM₁ composition pie graphs are proportional to the total PM₁ concentration for each air-mass cluster period, and the radius for the OA factor pie graphs is proportional to the total PM₁ organic concentration for each air-mass cluster period.

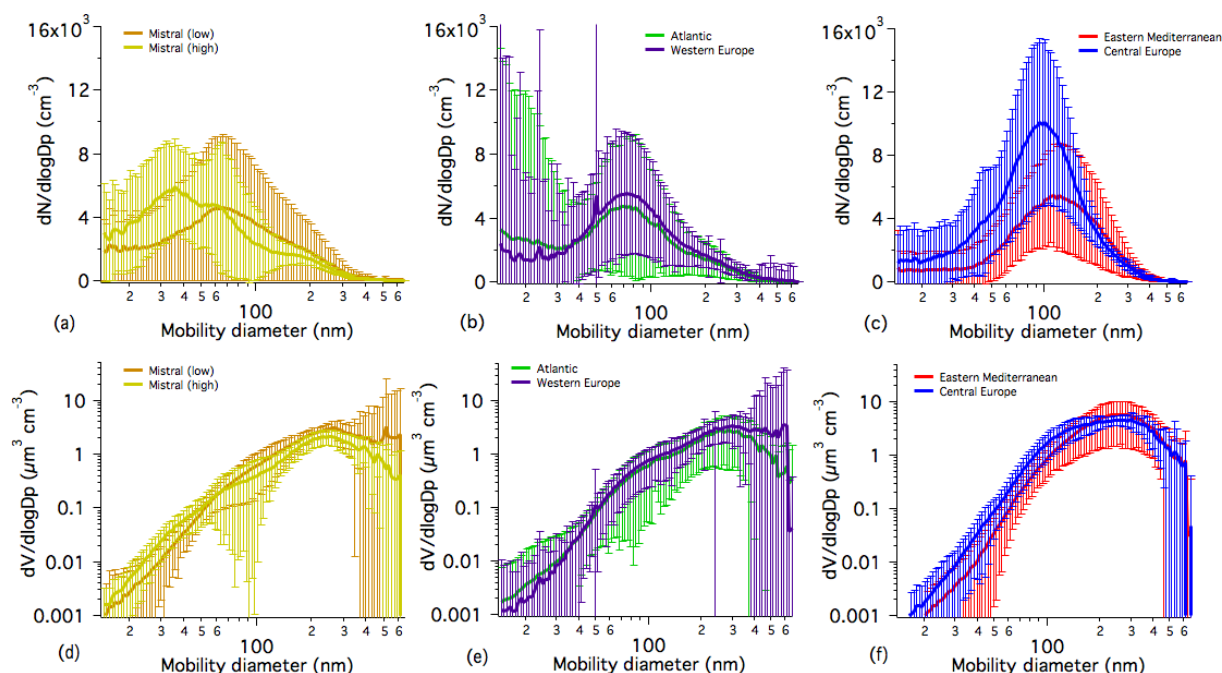


Figure 12. The number size distribution of PM₁ aerosol, coloured by averages for different air-mass origins: (a) mistral (high) and mistral (low); (b) Atlantic and western Europe; (c) eastern Mediterranean and central Europe; and the volume size distribution of PM₁ aerosol, coloured by averages for different air-mass origins: (d) mistral (high) and mistral (low); (e) Atlantic and western Europe; (f) eastern Mediterranean and central Europe.

There was only one period of mistral (high) air masses, spanning 38 h between 09:00 UTC on 24 June and 23:00 UTC on 25 June.

The most pronounced new particle formation (NPF) events and subsequent growth were observed during the two mistral air masses, particularly between 25 and 27 June. Very high number concentrations in the nucleation mode were also observed in very brief periods during the Atlantic and, to an extent, the western Europe air masses. There was no trend ($R^2 = 0.03$) over the whole campaign between the ratio of the particle number concentration between 14–25 nm and 14–600 nm and the fraction of CH_3SO_2^+ (a fragment of MSA, measured by the cToF-AMS) to total PM₁ organics (see Fig. S7). There was a weak positive trend during periods of the mistral (high) air mass ($R^2 = 0.39$). No trends were observed between the ratio of sub-25 nm and sub-600 nm particle number concentrations and the occurrence of other cToF-AMS fragments such as amines that could be linked with biogenic gas-to-particle conversion. Furthermore, there was a weak negative trend between the ratio of sub-25 nm and sub-600 nm particle number concentrations and the calculated f_{44} ($R^2 = 0.12$). Without instrumentation to measure the concentration of clusters and smaller aerosols (<14 nm) in conjunction with organic vapours over a longer time period, it is difficult to isolate and conclude the origin of these nucleation particles in a general sense, and we will limit our analysis to the most pronounced event during the campaign.

Figure 13 shows the size distribution over this period as well as SO_2 , eBC and CH_3SO_2^+ , as well as the back trajectory ending at 04:00 UTC on 25 June at Lampedusa. This NPF event occurred during the night and therefore in the absence of photochemistry. There was no discernible increase in eBC or SO_2 during these events and the 3 d cascade impactor sample from 25 to 28 June was characterized by the lowest concentrations of vanadium and nickel (released from heavy oil combustion events due to ship emissions) of the whole campaign. The air-mass back trajectory during this event was characteristic of the mistral (high) cluster. These are high-altitude air masses that descended over the Atlantic Ocean before having undergone a hydraulic jump over the southern France region and then a rapid descent over the western Mediterranean basin at high speed before arriving at the Lampedusa site. It is interesting to note that these air masses were anomalous for the typical June/July period at Lampedusa. Although the detected mass of CH_3SO_2^+ is likely due to the condensation of MSA on accumulation-mode particles, and considering that the cToF-AMS collection efficiency below ~ 100 nm is poor, the increasing concentration of CH_3SO_2^+ did coincide with the nucleation events during this period, suggesting a possible nucleation and condensation of marine biogenic vapours. Different studies indicate that NPF events may be triggered by atmospheric mixing processes (Kulmala et al., 2004; Hellmuth, 2006; Lauros et al., 2007, 2011) due to different phenomena like the enhance-

ment of turbulence in elevated layers (Wehner et al., 2010), the break-up of the nocturnal inversion (Stratmann et al., 2003) or the turbulence associated with the nocturnal low-level jet (Siebert et al., 2007). Nighttime NPF events have also been observed in the eastern Mediterranean (Kalivitis et al., 2012).

Furthermore, the intrusion of descending mid-tropospheric air masses in the boundary layer (Pace et al., 2015) has been linked to the occurrence of NPF events and would be consistent with the absence of high concentrations of BC, SO₂, vanadium and nickel which could be expected from ship emissions (Healy et al., 2009; Isakson et al., 2001) in the boundary layer over the Mediterranean. Pace et al. (2006) have shown that clean marine aerosol conditions are rare at Lampedusa and generally associated with north-westerly progressively descending trajectories, in agreement with the findings of this study. The relative absence of pre-existing particles acting as a condensation sink favours NPF events as observed during the field campaign.

3.6 Accumulation of sulfates across the Mediterranean

In order to investigate the ageing of aerosols across the north–south trajectory of European continental air masses, we compare the average NR-PM₁ composition measurements at Lampedusa to the concurrent measurements conducted at the Ersa site during summer 2013 (Michoud et al., 2017; Arndt et al., 2017). This is shown in Table 1.

On average, the PM₁ non-refractory organic mass concentrations at both sites were similar, with $\sim 3 \mu\text{g m}^{-3}$. NO₃⁻ concentrations were relatively small at both sites but higher at Ersa ($0.28 \mu\text{g m}^{-3}$) than at Lampedusa ($0.09 \mu\text{g m}^{-3}$). Sulfate concentrations were a factor of 3.2 times higher at Lampedusa ($4.5 \mu\text{g m}^{-3}$) than at Ersa ($1.4 \mu\text{g m}^{-3}$), while the ammonium concentrations were a factor of 2.7.

To investigate the possible accumulation of ammonium sulfate during the transport of air masses from Europe, the hourly air-mass back trajectories from Lampedusa were filtered so that only those that passed within $\pm 1^\circ$ latitude and longitude and within ± 200 m altitude of the station height of Ersa (550 m) were selected. These thresholds were chosen arbitrarily since there is no clear distinction in horizontal or vertical distance from the site that would necessarily constitute a representative air mass. This resulted in a total of 192 hourly observations at the Ersa site over 32 unique air-mass back-trajectory runs (see Fig. 14).

These trajectories were grouped mainly into the central Europe cluster ($n = 12$). The median trajectory duration between the Ersa and Lampedusa sites was 53 h, with a minimum of 33 h and a maximum of 144 h (corresponding to the total duration of the HYSPLIT model runs in this case). Those air masses grouped in the eastern Mediterranean cluster had the longest duration time between the sites of 127 h (while coincident with the Ersa site, these air masses still spent a significant amount of time over the eastern Mediter-

anean), followed by central Europe (83 h), western Europe (45 h) and then the mistral (low) (38 h). In general, between the two sites, there was a 40 % enhancement in the organic mass concentration but an increase in sulfate and ammonium by a factor of 6 and 4, respectively (Table 1).

The accumulation of (NH₄)₂SO₄ between Ersa and Lampedusa appeared to be dependent on the travel time of the air mass; however, different relationships were observed during different air-mass clusters. The total sulfate concentration at Lampedusa minus the total sulfate concentration at Ersa for the same air mass and accounting for the travel time as a function of the travel time is shown in Fig. 15.

There was a good positive correlation between the difference in sulfate concentrations between the two sites and the travel time for the central Europe and eastern Mediterranean air masses, while weak positive correlations were observed for the western Europe and mistral (low) clusters. It should be pointed out that the travel time was more than 110 h for the eastern Mediterranean air masses, while it was only between 33 and 58 h for the other three air-mass clusters. It is expected that the accumulation of sulfate would increase as the total travel time increases due to the opportunity for SO₂ conversion or from the addition of sulfate from separate air masses which are not accounted for in the HYSPLIT model. Although this relationship is somewhat demonstrated here, there are other factors that would influence the SO₄²⁻ accumulation. The sulfate concentrations presented here are measured by an Aerosol Chemical Speciation Monitor (ACSM) and cToF-AMS at the Ersa and Lampedusa sites, respectively. Both of these instruments have a 100 % inlet efficiency between ~ 100 and 800 nm. The conversion of SO₂ to SO₄²⁻ via nucleation and condensation is dependent on the pre-existing aerosol size distribution and condensation sink. Therefore, the use of PM₁ composition can be misleading if the sulfate is condensing on coarse particles. This is demonstrated in Fig. S2, which shows the size-resolved mass distribution of sulfur and sodium collected every 3 d on multi-stage cascade impactor filters; the relative contribution of sulfur in the PM₁ is higher than that of PM₁₀ in the absence of sodium (a tracer for sea salt). Furthermore, the concentrations of SO₄²⁻ measured by the PILS in the PM₁₀ fraction and cToF-AMS in the PM₁ are approximately equal with low sea salt concentrations ($\text{Na} + < 2 \mu\text{g m}^{-3}$) but are nearly a factor of 2 higher with the PILS for higher sea salt concentrations (Fig. S3). Furthermore, the emission of SO₂, typically from ships in the Mediterranean, is not necessarily constant over time and is likely not uniformly spread over the basin and within the vertical column (e.g. Becagli et al., 2017). This could possibly explain the discrepancy between the accumulation rate of sulfate between the eastern Mediterranean and central European air-mass origins. Moreover, the sample size for this analysis is relatively small and potentially not representative of the general accumulation of SO₄²⁻ but nonetheless they highlight the magnitude of accumulation under different air-mass trajectories.

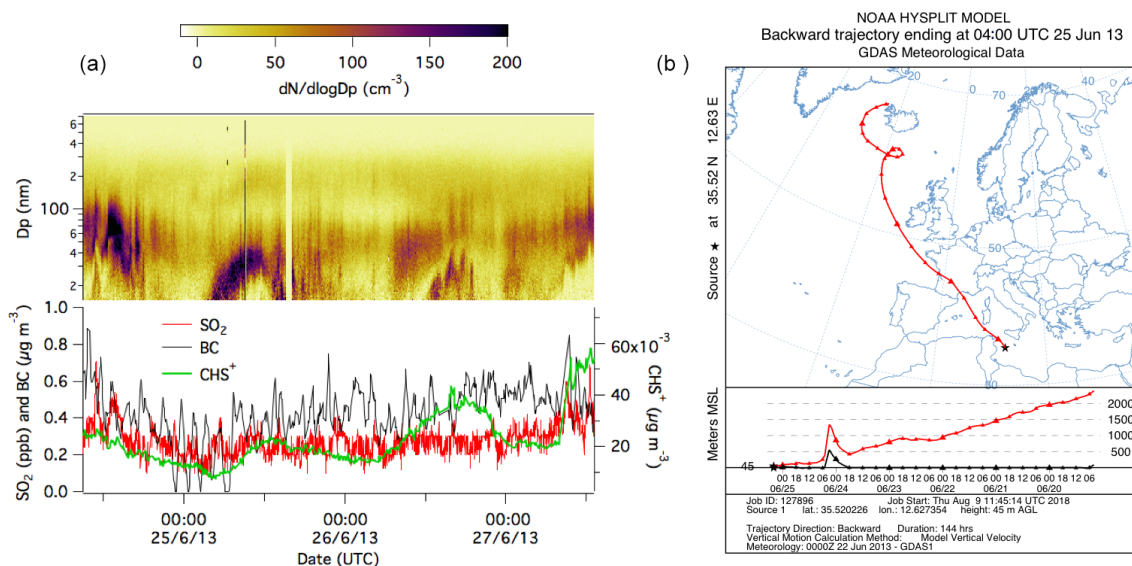


Figure 13. (a) The number size distribution during a new particle formation event on 25 June 2013 and the corresponding concentrations of SO₂, eBC and MSA fragment, CH₃SO₂⁺ and (b) the HYSPLIT air-mass back trajectory during the event.

Table 1. Campaign average PM₁ concentration for the major aerosol species measured at the Ersa and Lampedusa sites during the SOP-1a period and for periods of coincident air-mass back trajectories between Ersa and Lampedusa.

Site	SO ₄ ²⁻	Organic	NH ₄ ⁺	NO ₃ ⁻
Ersa	1.4 ± 2.6	3.0 ± 1.1	0.7 ± 1	0.3 ± 0.1
Lampedusa	4.5 ± 0.9	3.0 ± 1.6	1.9 ± 0.5	0.1 ± 0.2
Ersa (coincident with Lampedusa)	0.9 ± 0.5	2.7 ± 1.1	0.5 ± 0.3	0.4 ± 0.3
Lampedusa (coincident with Ersa)	5.3 ± 2.0	3.8 ± 0.8	2.0 ± 0.6	0.1 ± 0.1

4 Concluding remarks

The measurements carried out at Lampedusa during the ChArMEX/ADRIMED SOP-1a field campaign have provided a unique insight into the surface layer aerosols in the remote central Mediterranean. Air masses were influenced by transport from the eastern Mediterranean, central Europe, the western Europe, the Atlantic Ocean as well as western Europe. Air-mass clustering has been performed to explain observed differences in the aerosol composition and size at Lampedusa.

Hourly PM₁ mass ranged from 1.9 to 33.4 μg m⁻³, with an average of 10.2 μg m⁻³. It was composed on average of 41 % ± 9 % sulfate, 31 % ± 8 % organics, 17 % ± 3 % ammonium, 6 % ± 4 % black carbon, 1 % ± 0.4 % nitrate and 3 % ± 2 % sea salt. OA was highly oxidized ($f_{44} \sim 0.26$) and was apportioned to more oxidized oxygenated OA factor (MO-OOA, 53 %), less oxidized OOA factor (LO-OOA, 28 %), methanesulfonic acid OOA (MSA-OOA, 12 %) and

hydrogen-like OA (HOA, 8 %). The highest PM₁ mass loadings were observed for air masses from the eastern Mediterranean and central Europe, mostly due to the accumulation of ammonium and sulfate. Ancillary data from a remote site at the northern point of Cap Corse in the western Mediterranean showed increases of SO₄²⁻ concentrations between 2 and 12 μg m⁻³ when both sites (Corsica and Lampedusa) were connected. Apart from the dominance of ammonium sulfate on the PM₁ composition, the mass concentration and sources of OA have shown to be comparable to previous observations at European coastal and remote sites in the Mediterranean. The most pristine air masses, in terms of PM₁, were observed during periods with north-westerly winds which originated from the western Mediterranean or at high altitudes over the western European continent. Several nucleation and growth events, as well as large sea salt concentrations, were observed during these pristine periods. The largest concentrations of PM₁ were observed from air masses from central Europe and those that had circulated over the eastern Mediterranean.

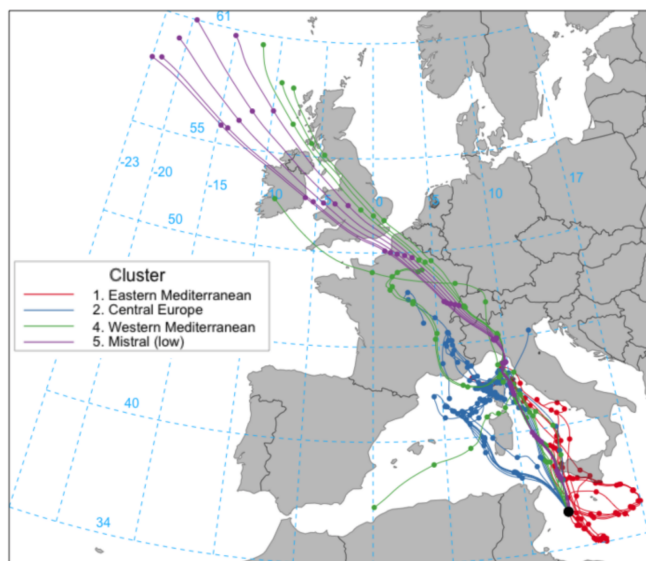


Figure 14. Hourly 120 h (5 d) back trajectories from Lampedusa that passed within $\pm 1^\circ$ in latitude and longitude and ± 200 m in altitude of the Ersa station. The colours represent the assigned cluster (performed on 144 h trajectories).

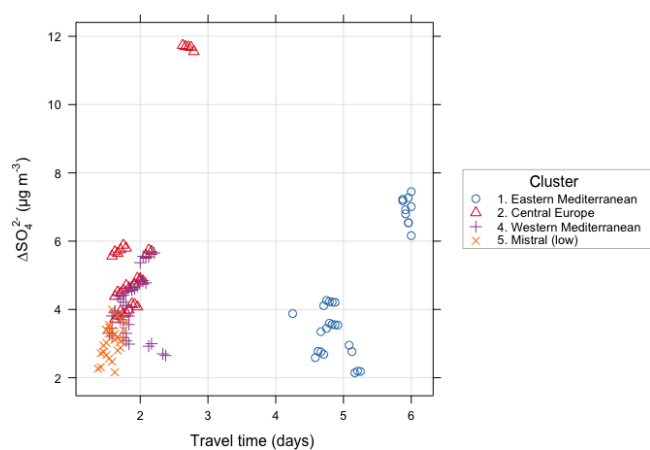


Figure 15. The difference in the PM₁ SO₄²⁻ mass concentration at Lampedusa and Ersa as a function of the travel time of the air masses from Ersa to Lampedusa. Colours represent the air-mass origin cluster.

In contrast to previous measurements of column-integrated aerosol optical properties (Pace et al., 2006; Meloni et al., 2006), we did not observe the presence of dust or biomass burning in the PM₁ range at the surface.

Our results also indicate a clear dichotomy of PM₁ aerosol composition from different source regions. Air masses from central Europe were characterized by a higher organic fraction than those from the eastern Mediterranean, which were enriched in sulfates. This difference could have potential implications on the optical properties and particularly the cloud condensation nuclei capabilities of those air masses. The rel-

ative occurrence of easterly air masses is not evident in the climatological wind roses nor in a previous study by Pace et al. (2006) that took a climatological approach of the air-mass back trajectories arriving at Lampedusa from 2001 to 2003. Nonetheless, a re-evaluation of the relative importance and occurrence of different air masses and aerosol properties should be undertaken.

Data availability. Open access to the data used for this publication is provided to registered users following the data and publication policy of the ChArMEx programme (http://mistrals.sedoo.fr/ChArMEx/Data-Policy/ChArMEx_DataPolicy.pdf; Sedoo, 2019). Additional code used in the analysis of data can be obtained upon request from the corresponding or first author. Weekly GDAS1 (Global Data Assimilation System; 1° resolution) analysis trajectory files were downloaded from the Air Resources Laboratory (ARL) of the National Oceanic and Atmospheric Administration (NOAA) archive (<ftp://arlftp.arlhq.noaa.gov/archives/gdas1/>; NOAA, 2018). The 144 h air-mass back trajectories were calculated using the R package, SplitR (<https://github.com/rich-iannone/SplitR>; Iannone, 2018). Cluster analyses were performed on these calculated trajectories, using the R package, OpenAir (Carslaw and Ropkins, 2012; data available at: <https://github.com/cran/openair>). Spectra used for comparison of PMF OA factors from those observed in other studies can be found at <http://cires.colorado.edu/jimenez-group/AMSSd/> (Ulbrich et al., 2018).

Supplement. The supplement related to this article is available online at: <https://doi.org/10.5194/acp-19-11123-2019-supplement>.

Author contributions. PF, BD, KD, JFD, AGdS designed the experiment in Lampedusa; JS designed the experiment in Ersa with contributions from coworkers. BD, AM, MCB, FC, GP, KD, CDB, JFD, MM, DM, JS, PZ, AGdS and PF performed the experiments. MDM, BD, AM, GP, KD, JS and PF analysed data, and all authors contributed to data interpretation. MDM, BD, GP, KD and PF wrote the manuscript with contributions and/or comments from all coauthors.

Competing interests. The authors declare that they have no conflict of interest.

Special issue statement. This article is part of the special issue “CHemistry and AeRosols Mediterranean EXperiments (ChArMEx) (ACP/AMT inter-journal SI)”. It is not associated with a conference.

Acknowledgements. This work is part of the ChArMEx project supported by CNRS-INSU, ADEME, Météo-France and CEA in the framework of the multidisciplinary programme MISTRALS (Mediterranean Integrated Studies at Regional And Local Scales; <http://mistrals-home.org/>, last access: 15 February 2019). Measure-

ments at Lampedusa were also supported by the Italian Ministry for University and Research through the NextData and RITMARE projects. The AERIS national data infrastructure is acknowledged for maintaining the ChArMEx database. Observations took place at the Roberto Sarao station (<http://www.lampedusa.enea.it/>, last access: 19 December 2018).

Financial support. This research has been supported by the French National Research Agency (grant no. ANR-11-BS56-0006).

Review statement. This paper was edited by Evangelos Gerasopoulos and reviewed by two anonymous referees.

References

- Aiken, A. C., Decarlo, P. F., Kroll, J. H., Worsnop, D. R., Huffman, J. A., Docherty, K. S., Ulbrich, I. M., Mohr, C., Kimmel, J. R., and Sueper, D.: *O/C* and *OM/OC* ratios of primary, secondary, and ambient organic aerosols with high-resolution time-of-flight aerosol mass spectrometry, *Environ. Sci. Technol.*, 42, 4478–4485, 2008.
- Allan, J. D., Jimenez, J. L., Williams, P. I., Alfarra, M. R., Bower, K. N., Jayne, J. T., Coe, H., and Worsnop, D. R.: Quantitative sampling using an Aerodyne aerosol mass spectrometer 1. Techniques of data interpretation and error analysis, *J. Geophys. Res.-Atmos.*, 108, 4090, <https://doi.org/10.1029/2002JD002358>, 2003.
- Amato, F., Alastuey, A., Karanasiou, A., Lucarelli, F., Nava, S., Calzolari, G., Severi, M., Becagli, S., Gianelle, V. L., Colombi, C., Alves, C., Custódio, D., Nunes, T., Cerqueira, M., Pio, C., Eleftheriadis, K., Diapouli, E., Reche, C., Minguillón, M. C., Manousakas, M.-I., Maggos, T., Vratolis, S., Harrison, R. M., and Querol, X.: AIRUSE-LIFE+: a harmonized PM speciation and source apportionment in five southern European cities, *Atmos. Chem. Phys.*, 16, 3289–3309, <https://doi.org/10.5194/acp-16-3289-2016>, 2016.
- Ancellet, G., Pelon, J., Totems, J., Chazette, P., Bazureau, A., Sicard, M., Di Iorio, T., Dulac, F., and Mallet, M.: Long-range transport and mixing of aerosol sources during the 2013 North American biomass burning episode: analysis of multiple lidar observations in the western Mediterranean basin, *Atmos. Chem. Phys.*, 16, 4725–4742, <https://doi.org/10.5194/acp-16-4725-2016>, 2016.
- Arndt, J., Sciare, J., Mallet, M., Roberts, G. C., Marchand, N., Sartelet, K., Sellegri, K., Dulac, F., Healy, R. M., and Wenger, J. C.: Sources and mixing state of summertime background aerosol in the north-western Mediterranean basin, *Atmos. Chem. Phys.*, 17, 6975–7001, <https://doi.org/10.5194/acp-17-6975-2017>, 2017.
- Becagli, S., Sferlazzo, D. M., Pace, G., di Sarra, A., Bommarito, C., Calzolari, G., Ghedini, C., Lucarelli, F., Meloni, D., Monteleone, F., Severi, M., Traversi, R., and Udisti, R.: Evidence for heavy fuel oil combustion aerosols from chemical analyses at the island of Lampedusa: a possible large role of ships emissions in the Mediterranean, *Atmos. Chem. Phys.*, 12, 3479–3492, <https://doi.org/10.5194/acp-12-3479-2012>, 2012.
- Becagli, S., Anello, F., Bommarito, C., Cassola, F., Calzolari, G., Di Iorio, T., di Sarra, A., Gómez-Amo, J.-L., Lucarelli, F., Marconi, M., Meloni, D., Monteleone, F., Nava, S., Pace, G., Severi, M., Sferlazzo, D. M., Traversi, R., and Udisti, R.: Constraining the ship contribution to the aerosol of the central Mediterranean, *Atmos. Chem. Phys.*, 17, 2067–2084, <https://doi.org/10.5194/acp-17-2067-2017>, 2017.
- Bougiatioti, A., Stavroulas, I., Kostenidou, E., Zampas, P., Theodosi, C., Kouvarakis, G., Canonaco, F., Prévôt, A. S. H., Nenes, A., Pandis, S. N., and Mihalopoulos, N.: Processing of biomass-burning aerosol in the eastern Mediterranean during summertime, *Atmos. Chem. Phys.*, 14, 4793–4807, <https://doi.org/10.5194/acp-14-4793-2014>, 2014.
- Bove, M., Brotto, P., Calzolari, G., Cassola, F., Cavalli, F., Fermo, P., Hjorth, J., Massabò, D., Nava, S., and Piazzalunga, A.: PM₁₀ source apportionment applying PMF and chemical tracer analysis to ship-borne measurements in the Western Mediterranean, *Atmos. Environ.*, 125, 140–151, 2016.
- Bozzetti, C., El Haddad, I., Salameh, D., Daellenbach, K. R., Fermo, P., Gonzalez, R., Minguillón, M. C., Iinuma, Y., Poulain, L., Elser, M., Müller, E., Slowik, J. G., Jaffrezou, J.-L., Baltensperger, U., Marchand, N., and Prévôt, A. S. H.: Organic aerosol source apportionment by offline-AMS over a full year in Marseille, *Atmos. Chem. Phys.*, 17, 8247–8268, <https://doi.org/10.5194/acp-17-8247-2017>, 2017.
- Brocchi, V., Krysztofiak, G., Catoire, V., Guth, J., Marécal, V., Zbinden, R., El Amraoui, L., Dulac, F., and Ricaud, P.: Intercontinental transport of biomass burning pollutants over the Mediterranean Basin during the summer 2014 ChArMEx-GLAM airborne campaign, *Atmos. Chem. Phys.*, 18, 6887–6906, <https://doi.org/10.5194/acp-18-6887-2018>, 2018.
- Calzolari, G., Nava, S., Lucarelli, F., Chiari, M., Giannoni, M., Becagli, S., Traversi, R., Marconi, M., Frosini, D., Severi, M., Udisti, R., di Sarra, A., Pace, G., Meloni, D., Bommarito, C., Monteleone, F., Anello, F., and Sferlazzo, D. M.: Characterization of PM₁₀ sources in the central Mediterranean, *Atmos. Chem. Phys.*, 15, 13939–13955, <https://doi.org/10.5194/acp-15-13939-2015>, 2015.
- Carslaw, D. C. and Ropkins, K.: Openair – an R package for air quality data analysis, *Environ. Modell. Softw.*, 27, 52–61, <https://doi.org/10.1016/j.envsoft.2011.09.008>, 2012 (data available at: <https://github.com/cran/openair>, last access: 30 May 2018).
- Chang, R. Y.-W., Leck, C., Graus, M., Müller, M., Paatero, J., Burkhardt, J. F., Stohl, A., Orr, L. H., Hayden, K., Li, S.-M., Hansel, A., Tjernström, M., Leaitch, W. R., and Abbatt, J. P. D.: Aerosol composition and sources in the central Arctic Ocean during ASCOS, *Atmos. Chem. Phys.*, 11, 10619–10636, <https://doi.org/10.5194/acp-11-10619-2011>, 2011.
- Chrit, M., Sartelet, K., Sciare, J., Pey, J., Marchand, N., Couvidat, F., Sellegri, K., and Beekmann, M.: Modelling organic aerosol concentrations and properties during ChArMEx summer campaigns of 2012 and 2013 in the western Mediterranean region, *Atmos. Chem. Phys.*, 17, 12509–12531, <https://doi.org/10.5194/acp-17-12509-2017>, 2017.
- Chrit, M., Sartelet, K., Sciare, J., Pey, J., Nicolas, J. B., Marchand, N., Freney, E., Sellegri, K., Beekmann, M., and Dulac, F.: Aerosol sources in the western Mediterranean during summer-

- time: a model-based approach, *Atmos. Chem. Phys.*, 18, 9631–9659, <https://doi.org/10.5194/acp-18-9631-2018>, 2018.
- Crippa, M., DeCarlo, P. F., Slowik, J. G., Mohr, C., Heringa, M. F., Chirico, R., Poulain, L., Freutel, F., Sciare, J., Cozic, J., Di Marco, C. F., Elsasser, M., Nicolas, J. B., Marchand, N., Abidi, E., Wiedensohler, A., Drewnick, F., Schneider, J., Borrmann, S., Nemitz, E., Zimmermann, R., Jaffrezo, J.-L., Prévôt, A. S. H., and Baltensperger, U.: Wintertime aerosol chemical composition and source apportionment of the organic fraction in the metropolitan area of Paris, *Atmos. Chem. Phys.*, 13, 961–981, <https://doi.org/10.5194/acp-13-961-2013>, 2013.
- Crippa, M., Canonaco, F., Lanz, V. A., Äijälä, M., Allan, J. D., Carbone, S., Capes, G., Ceburnis, D., Dall'Osto, M., Day, D. A., DeCarlo, P. F., Ehn, M., Eriksson, A., Freney, E., Hildebrandt Ruiz, L., Hillamo, R., Jimenez, J. L., Junninen, H., Kiendler-Scharr, A., Kortelainen, A.-M., Kulmala, M., Laaksonen, A., Mensah, A. A., Mohr, C., Nemitz, E., O'Dowd, C., Ovadnevaite, J., Pandis, S. N., Petäjä, T., Poulain, L., Saarikoski, S., Sellegri, K., Swietlicki, E., Tiitta, P., Worsnop, D. R., Baltensperger, U., and Prévôt, A. S. H.: Organic aerosol components derived from 25 AMS data sets across Europe using a consistent ME-2 based source apportionment approach, *Atmos. Chem. Phys.*, 14, 6159–6176, <https://doi.org/10.5194/acp-14-6159-2014>, 2014.
- Denjean, C., Cassola, F., Mazzino, A., Triquet, S., Chevillier, S., Grand, N., Bourriane, T., Momboisse, G., Sellegri, K., Schwarzenbock, A., Freney, E., Mallet, M., and Formenti, P.: Size distribution and optical properties of mineral dust aerosols transported in the western Mediterranean, *Atmos. Chem. Phys.*, 16, 1081–1104, <https://doi.org/10.5194/acp-16-1081-2016>, 2016.
- Diapouli, E., Manousakas, M. I., Vratolis, S., Vasilatou, V., Pateraki, S., Bairachtari, K. A., Querol, X., Amato, F., Alastuey, A., Karanasiou, A. A., Lucarelli, F., Nava, S., Calzolari, G., Gianelle, V. L., Colombi, C., Alves, C., Custódio, D., Pio, C., Spyrou, C., Kallos, G. B., and Eleftheriadis, K.: AIRUSE-LIFE+: estimation of natural source contributions to urban ambient air PM₁₀ and PM_{2.5} concentrations in southern Europe – implications to compliance with limit values, *Atmos. Chem. Phys.*, 17, 3673–3685, <https://doi.org/10.5194/acp-17-3673-2017>, 2017.
- Drewnick, F., Hings, S. S., DeCarlo, P., Jayne, J. T., Gonin, M., Fuhrer, K., Weimer, S., Jimenez, J. L., Demerjian, K. L., and Borrmann, S.: A new time-of-flight aerosol mass spectrometer (TOF-AMS) – Instrument description and first field deployment, *Aerosol. Sci. Tech.*, 39, 637–658, 2005.
- Drewnick, F., Hings, S. S., Alfarra, M. R., Prevot, A. S. H., and Borrmann, S.: Aerosol quantification with the Aerodyne Aerosol Mass Spectrometer: detection limits and ionizer background effects, *Atmos. Meas. Tech.*, 2, 33–46, <https://doi.org/10.5194/amt-2-33-2009>, 2009.
- El Haddad, I., D'Anna, B., Temime-Roussel, B., Nicolas, M., Boreave, A., Favez, O., Voisin, D., Sciare, J., George, C., Jaffrezo, J.-L., Wortham, H., and Marchand, N.: Towards a better understanding of the origins, chemical composition and aging of oxygenated organic aerosols: case study of a Mediterranean industrialized environment, Marseille, *Atmos. Chem. Phys.*, 13, 7875–7894, <https://doi.org/10.5194/acp-13-7875-2013>, 2013.
- Formenti, P., Boucher, O., Reiner, T., Sprung, D., Andreae, M. O., Wendisch, M., Wex, H., Kindred, D., Tzortziou, M., and Vasaras, A.: STAAARTE-MED 1998 summer airborne measurements over the Aegean Sea 2. Aerosol scattering and absorption, and radiative calculations, *J. Geophys. Res.-Atmos.*, 107, 4451, <https://doi.org/10.1029/2001JD001536>, 2002.
- Formenti, P., Mbemba Kabuiku, L., Chiapello, I., Ducos, F., Dulac, F., and Tanré, D.: Aerosol optical properties derived from POLDER-3/PARASOL (2005–2013) over the western Mediterranean Sea – Part 1: Quality assessment with AERONET and in situ airborne observations, *Atmos. Meas. Tech.*, 11, 6761–6784, <https://doi.org/10.5194/amt-11-6761-2018>, 2018.
- Ghahremaninezhad, R., Norman, A.-L., Abbatt, J. P. D., Levasseur, M., and Thomas, J. L.: Biogenic, anthropogenic and sea salt sulfate size-segregated aerosols in the Arctic summer, *Atmos. Chem. Phys.*, 16, 5191–5202, <https://doi.org/10.5194/acp-16-5191-2016>, 2016.
- Haywood, J. and Boucher, O.: Estimates of the direct and indirect radiative forcing due to tropospheric aerosols: A review, *Rev. Geophys.*, 38, 513–543, 2000.
- Healy, R. M., O'Connor, I. P., Hellebust, S., Allanic, A., Sodeau, J. R., and Wenger, J. C.: Characterisation of single particles from in-port ship emissions, *Atmos. Environ.*, 43, 6408–6414, 2009.
- Hellmuth, O.: Columnar modelling of nucleation burst evolution in the convective boundary layer – first results from a feasibility study Part IV: A compilation of previous observations for valuation of simulation results from a columnar modelling study, *Atmos. Chem. Phys.*, 6, 4253–4274, <https://doi.org/10.5194/acp-6-4253-2006>, 2006.
- Hersey, S. P., Craven, J. S., Schilling, K. A., Metcalf, A. R., Sorooshian, A., Chan, M. N., Flagan, R. C., and Seinfeld, J. H.: The Pasadena Aerosol Characterization Observatory (PACO): chemical and physical analysis of the Western Los Angeles basin aerosol, *Atmos. Chem. Phys.*, 11, 7417–7443, <https://doi.org/10.5194/acp-11-7417-2011>, 2011.
- Hildebrandt, L., Engelhart, G. J., Mohr, C., Kostenidou, E., Lanz, V. A., Bougiatioti, A., DeCarlo, P. F., Prevot, A. S. H., Baltensperger, U., Mihalopoulos, N., Donahue, N. M., and Pandis, S. N.: Aged organic aerosol in the Eastern Mediterranean: the Finokalia Aerosol Measurement Experiment – 2008, *Atmos. Chem. Phys.*, 10, 4167–4186, <https://doi.org/10.5194/acp-10-4167-2010>, 2010.
- Hildebrandt, L., Kostenidou, E., Lanz, V. A., Prevot, A. S. H., Baltensperger, U., Mihalopoulos, N., Laaksonen, A., Donahue, N. M., and Pandis, S. N.: Sources and atmospheric processing of organic aerosol in the Mediterranean: insights from aerosol mass spectrometer factor analysis, *Atmos. Chem. Phys.*, 11, 12499–12515, <https://doi.org/10.5194/acp-11-12499-2011>, 2011.
- Iannone, R.: SplitR: Use the HYSPLIT model inside R and do more with it, available at: <https://github.com/rich-iannone/SplitR>, last access: 18 May 2018.
- Isakson, J., Persson, T. A., and Lindgren, E. S.: Identification and assessment of ship emissions and their effects in the harbour of Göteborg, Sweden, *Atmos. Environ.*, 35, 3659–3666, 2001.
- Jimenez, J. L., Canagaratna, M., Donahue, N., Prevot, A., Zhang, Q., Kroll, J. H., DeCarlo, P. F., Allan, J. D., Coe, H., and Ng, N.: Evolution of organic aerosols in the atmosphere, *Science*, 326, 1525–1529, 2009.
- Kalivitis, N., Stavroulas, I., Bougiatioti, A., Kouvarakis, G., Gagné, S., Manninen, H. E., Kulmala, M., and Mihalopoulos, N.: Night-time enhanced atmospheric ion concentrations in the

- marine boundary layer, *Atmos. Chem. Phys.*, 12, 3627–3638, <https://doi.org/10.5194/acp-12-3627-2012>, 2012.
- Kalnay, E., Kanamitsu, M., Kistler, R., Collins, W., Deaven, D., Gandin, L., Iredell, M., Saha, S., White, G., Woollen, J., Zhu, Y., Chelliah, M., Ebisuzaki, W., Higgins, W., Janowiak, J., Mo, K. C., Ropelewski, C., Wang, J., Leetmaa, A., Reynolds, R., Jenne, R., and Joseph, D.: The NCEP/NCAR 40-year reanalysis project, *B. Am. Meteorol. Soc.*, 77, 437–471, 1996.
- Koçak, M., Mihalopoulos, N., and Kubilay, N.: Chemical composition of the fine and coarse fraction of aerosols in the northeastern Mediterranean, *Atmos. Environ.*, 41, 7351–7368, 2007.
- Koulouri, E., Saarikoski, S., Theodosi, C., Markaki, Z., Gerasopoulos, E., Kouvarakis, G., Mäkelä, T., Hillamo, R., and Mihalopoulos, N.: Chemical composition and sources of fine and coarse aerosol particles in the Eastern Mediterranean, *Atmos. Environ.*, 42, 6542–6550, 2008.
- Kulmala, M., Vehkamäki, H., Petäjä, T., Dal Maso, M., Lauri, A., Kerminen, V.-M., Birmili, W., and McMurry, P.: Formation and growth rates of ultrafine atmospheric particles: a review of observations, *J. Aerosol. Sci.*, 35, 143–176, 2004.
- Lanz, V. A., Alfara, M. R., Baltensperger, U., Buchmann, B., Hueglin, C., Szidat, S., Wehrli, M. N., Wacker, L., Weimer, S., and Caseiro, A.: Source attribution of submicron organic aerosols during wintertime inversions by advanced factor analysis of aerosol mass spectra, *Environ. Sci. Technol.*, 42, 214–220, 2007.
- Lauros, J., Nilsson, E. D., Dal Maso, M., and Kulmala, M.: Contribution of mixing in the ABL to new particle formation based on observations, *Atmos. Chem. Phys.*, 7, 4781–4792, <https://doi.org/10.5194/acp-7-4781-2007>, 2007.
- Lauros, J., Sogachev, A., Smolander, S., Vuollekoski, H., Sihto, S.-L., Mammarella, I., Laakso, L., Rannik, Ü., and Boy, M.: Particle concentration and flux dynamics in the atmospheric boundary layer as the indicator of formation mechanism, *Atmos. Chem. Phys.*, 11, 5591–5601, <https://doi.org/10.5194/acp-11-5591-2011>, 2011.
- Lelieveld, J., Berresheim, H., Borrmann, S., Crutzen, P., Dentener, F., Fischer, H., Feichter, J., Flatau, P., Heland, J., and Holzinger, R.: Global air pollution crossroads over the Mediterranean, *Science*, 298, 794–799, 2002.
- Mallet, M., Dulac, F., Formenti, P., Nabat, P., Sciare, J., Roberts, G., Pelon, J., Ancellet, G., Tanré, D., Parol, F., Denjean, C., Brogniez, G., di Sarra, A., Alados-Arboledas, L., Arndt, J., Auriol, F., Blarel, L., Bourriane, T., Chazette, P., Chevaillier, S., Claeys, M., D’Anna, B., Derimian, Y., Desboeufs, K., Di Iorio, T., Doussin, J.-F., Durand, P., Féron, A., Freney, E., Gaimoz, C., Goloub, P., Gómez-Amo, J. L., Granados-Muñoz, M. J., Grand, N., Hamonou, E., Jankowiak, I., Jeannot, M., Léon, J.-F., Maillé, M., Mailler, S., Meloni, D., Menut, L., Mombouisse, G., Nicolas, J., Podvin, T., Pont, V., Rea, G., Renard, J.-B., Roblou, L., Schepanski, K., Schwarzenboeck, A., Sellegri, K., Sicard, M., Solmon, F., Somot, S., Torres, B., Totems, J., Triquet, S., Verdier, N., Verwaerde, C., Waquet, F., Wenger, J., and Zapf, P.: Overview of the Chemistry-Aerosol Mediterranean Experiment/Aerosol Direct Radiative Forcing on the Mediterranean Climate (ChArMEx/ADRMED) summer 2013 campaign, *Atmos. Chem. Phys.*, 16, 455–504, <https://doi.org/10.5194/acp-16-455-2016>, 2016.
- Mariotti, A., Pan, Y., Zeng, N., and Alessandri, A.: Long-term climate change in the Mediterranean region in the midst of decadal variability, *Clim. Dynam.*, 44, 1437–1456, 2015.
- Marple, V. A., Rubow, K. L., and Behm, S. M.: A Microorifice Uniform Deposit Impactor (MOUDI): Description, Calibration, and Use, *Aerosol Sci. Tech.*, 14, 434–446, <https://doi.org/10.1080/02786829108959504>, 1991.
- Meloni, D., di Sarra, A., Pace, G., and Monteleone, F.: Aerosol optical properties at Lampedusa (Central Mediterranean). 2. Determination of single scattering albedo at two wavelengths for different aerosol types, *Atmos. Chem. Phys.*, 6, 715–727, <https://doi.org/10.5194/acp-6-715-2006>, 2006.
- Michoud, V., Sciare, J., Sauvage, S., Dusanter, S., Léonardis, T., Gros, V., Kalogridis, C., Zannoni, N., Féron, A., Petit, J.-E., Crenn, V., Baisnée, D., Sarda-Estève, R., Bonnaire, N., Marchand, N., DeWitt, H. L., Pey, J., Colomb, A., Gheusi, F., Szidat, S., Stavroulas, I., Borbon, A., and Locoge, N.: Organic carbon at a remote site of the western Mediterranean Basin: sources and chemistry during the ChArMEx SOP2 field experiment, *Atmos. Chem. Phys.*, 17, 8837–8865, <https://doi.org/10.5194/acp-17-8837-2017>, 2017.
- Middlebrook, A., Bahreini, R., Jimenez, J., and Canagaratna, M.: Evaluation of composition-dependent collection efficiencies for the aerodyne aerosol mass spectrometer using field data, *Aerosol Sci. Tech.*, 46, 258–271, <https://doi.org/10.1080/02786826.2011.620041>, 2012.
- Minguillón, M., Pérez, N., Marchand, N., Bertrand, A., Temime-Roussel, B., Agrios, K., Szidat, S., van Drooge, B., Sylvestre, A., and Alastuey, A.: Secondary organic aerosol origin in an urban environment: influence of biogenic and fuel combustion precursors, *Faraday Discuss.*, 189, 337–359, 2016.
- Minguillón, M. C., Ripoll, A., Pérez, N., Prévôt, A. S. H., Canonaco, F., Querol, X., and Alastuey, A.: Chemical characterization of submicron regional background aerosols in the western Mediterranean using an Aerosol Chemical Speciation Monitor, *Atmos. Chem. Phys.*, 15, 6379–6391, <https://doi.org/10.5194/acp-15-6379-2015>, 2015.
- Mohr, C., DeCarlo, P. F., Heringa, M. F., Chirico, R., Slowik, J. G., Richter, R., Reche, C., Alastuey, A., Querol, X., Seco, R., Peñuelas, J., Jiménez, J. L., Crippa, M., Zimmermann, R., Baltensperger, U., and Prévôt, A. S. H.: Identification and quantification of organic aerosol from cooking and other sources in Barcelona using aerosol mass spectrometer data, *Atmos. Chem. Phys.*, 12, 1649–1665, <https://doi.org/10.5194/acp-12-1649-2012>, 2012.
- Muller, M., George, C., and D’Anna, B.: Enhanced spectral analysis of C-TOF Aerosol Mass Spectrometer data: iterative residual analysis and cumulative peak fitting, *Int. J. Mass. Spectrom.*, 306, 1–8, 2011.
- Ng, N. L., Canagaratna, M. R., Zhang, Q., Jimenez, J. L., Tian, J., Ulbrich, I. M., Kroll, J. H., Docherty, K. S., Chhabra, P. S., Bahreini, R., Murphy, S. M., Seinfeld, J. H., Hildebrandt, L., Donahue, N. M., DeCarlo, P. F., Lanz, V. A., Prévôt, A. S. H., Dinar, E., Rudich, Y., and Worsnop, D. R.: Organic aerosol components observed in Northern Hemispheric datasets from Aerosol Mass Spectrometry, *Atmos. Chem. Phys.*, 10, 4625–4641, <https://doi.org/10.5194/acp-10-4625-2010>, 2010.
- Ng, N. L., Canagaratna, M. R., Jimenez, J. L., Chhabra, P. S., Seinfeld, J. H., and Worsnop, D. R.: Changes in organic aerosol

- composition with aging inferred from aerosol mass spectra, *Atmos. Chem. Phys.*, 11, 6465–6474, <https://doi.org/10.5194/acp-11-6465-2011>, 2011.
- NOAA: Global Data Assimilation System 1 data archive, available at: <ftp://arlftp.arlhq.noaa.gov/archives/gdas1/>, last access: 18 May 2018.
- Orsini, D. A., Ma, Y., Sullivan, A., Sierau, B., Baumann, K., and Weber, R. J.: Refinements to the particle-into-liquid sampler (PILS) for ground and airborne measurements of water soluble aerosol composition, *Atmos. Environ.*, 37, 1243–1259, 2003.
- Ortiz-Amezcuca, P., Guerrero-Rascado, J., Granados-Muñoz, M., Bravo-Aranda, J., and Alados-Arboledas, L.: Characterization of atmospheric aerosols for a long range transport of biomass burning particles from canadian forest fires over the southern iberian peninsula in July 2013, *Optica Pura y Aplicada*, 47, 43–49, 2014.
- Ovadnevaite, J., Ceburnis, D., Canagaratna, M., Berresheim, H., Bialek, J., Martucci, G., Worsnop, D. R., and O’Dowd, C.: On the effect of wind speed on submicron sea salt mass concentrations and source fluxes, *J. Geophys. Res.*, 117, D16201, <https://doi.org/10.1029/2011JD017379>, 2012.
- Paatero, P.: Least squares formulation of robust non-negative factor analysis, *Chemometr. Intell. Lab.*, 37, 23–35, 1997.
- Paatero, P. and Tapper, U.: Positive matrix factorization: A non-negative factor model with optimal utilization of error estimates of data values, *Environmetrics*, 5, 111–126, 1994.
- Pace, G., Meloni, D., and di Sarra, A.: Forest fire aerosol over the Mediterranean basin during summer 2003, *J. Geophys. Res.-Atmos.*, 110, D21202, <https://doi.org/10.1029/2005JD005986>, 2005.
- Pace, G., di Sarra, A., Meloni, D., Piacentino, S., and Chamard, P.: Aerosol optical properties at Lampedusa (Central Mediterranean). 1. Influence of transport and identification of different aerosol types, *Atmos. Chem. Phys.*, 6, 697–713, <https://doi.org/10.5194/acp-6-697-2006>, 2006.
- Perrone, M. and Bergamo, A.: Direct radiative forcing during Sahara dust intrusions at a site in the Central Mediterranean: Anthropogenic particle contribution, *Atmos. Res.*, 101, 783–798, 2011.
- Perrone, M., Becagli, S., Orza, J. G., Vecchi, R., Dinoi, A., Udisti, R., and Cabello, M.: The impact of long-range-transport on PM₁ and PM_{2.5} at a Central Mediterranean site, *Atmos. Environ.*, 71, 176–186, 2013.
- Petit, J.-E., Favez, O., Albinet, A., and Canonaco, F.: A user-friendly tool for comprehensive evaluation of the geographical origins of atmospheric pollution: Wind and trajectory analyses, *Environ. Modell. Softw.*, 88, 183–187, 2017.
- Pikridas, M., Riipinen, I., Hildebrandt, L., Kostenidou, E., Manninen, H., Mihalopoulos, N., Kalivitis, N., Burkhardt, J. F., Stohl, A., and Kulmala, M.: New particle formation at a remote site in the eastern Mediterranean, *J. Geophys. Res.*, 117, D12205, <https://doi.org/10.1029/2012JD017570>, 2012.
- Querol, X., Alastuey, A., Pey, J., Cusack, M., Pérez, N., Mihalopoulos, N., Theodosi, C., Gerasopoulos, E., Kubilay, N., and Koçak, M.: Variability in regional background aerosols within the Mediterranean, *Atmos. Chem. Phys.*, 9, 4575–4591, <https://doi.org/10.5194/acp-9-4575-2009>, 2009a.
- Querol, X., Pey, J., Pandolfi, M., Alastuey, A., Cusack, M., Pérez, N., Moreno, T., Viana, M., Mihalopoulos, N., and Kallos, G.: African dust contributions to mean ambient PM₁₀ mass-levels across the Mediterranean Basin, *Atmos. Environ.*, 43, 4266–4277, 2009b.
- Rinaldi, M., Gilardoni, S., Paglione, M., Sandrini, S., Decesari, S., Zanca, N., Marinoni, A., Cristofanelli, P., Bonasoni, P., and Ielpo, P.: Physico-chemical characterization of Mediterranean background aerosol at the Capogranitola observatory (Sicily), EGU General Assembly Conference Abstracts, 23–28 April 2017, Vienna, Austria, 3161, 2017.
- Sanchez-Gomez, E., Somot, S., and Mariotti, A.: Future changes in the Mediterranean water budget projected by an ensemble of regional climate models, *Geophys. Res. Lett.*, 36, L21401, <https://doi.org/10.1029/2009GL040120>, 2009.
- Schembari, C., Bove, M., Cuccia, E., Cavalli, F., Hjorth, J., Massabò, D., Nava, S., Udisti, R., and Prati, P.: Source apportionment of PM₁₀ in the Western Mediterranean based on observations from a cruise ship, *Atmos. Environ.*, 98, 510–518, 2014.
- Schmale, J., Schneider, J., Nemitz, E., Tang, Y. S., Dragosits, U., Blackall, T. D., Trathan, P. N., Phillips, G. J., Sutton, M., and Braban, C. F.: Sub-Antarctic marine aerosol: dominant contributions from biogenic sources, *Atmos. Chem. Phys.*, 13, 8669–8694, <https://doi.org/10.5194/acp-13-8669-2013>, 2013.
- Sciare, J., Bardouki, H., Moulin, C., and Mihalopoulos, N.: Aerosol sources and their contribution to the chemical composition of aerosols in the Eastern Mediterranean Sea during summertime, *Atmos. Chem. Phys.*, 3, 291–302, <https://doi.org/10.5194/acp-3-291-2003>, 2003.
- Sciare, J., Oikonomou, K., Favez, O., Liakakou, E., Markaki, Z., Cachier, H., and Mihalopoulos, N.: Long-term measurements of carbonaceous aerosols in the Eastern Mediterranean: evidence of long-range transport of biomass burning, *Atmos. Chem. Phys.*, 8, 5551–5563, <https://doi.org/10.5194/acp-8-5551-2008>, 2008.
- Sedoo: ChArMEX database Data Policy, available at: http://mistrals.sedoo.fr/ChArMEX/Data-Policy/ChArMEX_DataPolicy.pdf, last access: 16 June 2018.
- Siebert, H., Wehner, B., Hellmuth, O., Stratmann, F., Boy, M., and Kulmala, M.: New-particle formation in connection with a nocturnal low-level jet: Observations and modeling results, *Geophys. Res. Lett.*, 34, L16822, <https://doi.org/10.1029/2007GL029891>, 2007.
- Sirois, A. and Bottenheim, J. W.: Use of backward trajectories to interpret the 5-year record of PAN and O₃ ambient air concentrations at Kejimikujik National Park, Nova Scotia, *J. Geophys. Res.-Atmos.*, 100, 2867–2881, 1995.
- Stein, A., Draxler, R. R., Rolph, G. D., Stunder, B. J., Cohen, M., and Ngan, F.: NOAA’s HYSPLIT atmospheric transport and dispersion modeling system, *B. Am. Meteorol. Soc.*, 96, 2059–2077, 2015.
- Stohl, A., Forster, C., Frank, A., Seibert, P., and Wotawa, G.: Technical note: The Lagrangian particle dispersion model FLEXPART version 6.2, *Atmos. Chem. Phys.*, 5, 2461–2474, <https://doi.org/10.5194/acp-5-2461-2005>, 2005.
- Stratmann, F., Siebert, H., Spindler, G., Wehner, B., Althausen, D., Heintzenberg, J., Hellmuth, O., Rinke, R., Schmieder, U., Seidel, C., Tuch, T., Uhrner, U., Wiedensohler, A., Wandinger, U., Wendisch, M., Schell, D., and Stohl, A.: New-particle formation events in a continental boundary layer: first results from the SATURN experiment, *Atmos. Chem. Phys.*, 3, 1445–1459, <https://doi.org/10.5194/acp-3-1445-2003>, 2003.

- Tadros, C. V., Crawford, J., Treble, P. C., Baker, A., Cohen, D. D., Atanacio, A. J., Hankin, S., and Roach, R.: Chemical characterisation and source identification of atmospheric aerosols in the Snowy Mountains, south-eastern Australia, *Sci. Total Environ.*, 630, 432–443, 2018.
- Ulbrich, I. M., Canagaratna, M. R., Zhang, Q., Worsnop, D. R., and Jimenez, J. L.: Interpretation of organic components from Positive Matrix Factorization of aerosol mass spectrometric data, *Atmos. Chem. Phys.*, 9, 2891–2918, <https://doi.org/10.5194/acp-9-2891-2009>, 2009.
- Ulbrich, I. M., Handschy, A., Lechner, M., and Jimenez, J. L.: AMS Spectral Database, available at: <http://cires.colorado.edu/jimenez-group/AMSsd>, last access: 18 November 2018.
- Wehner, B., Siebert, H., Ansmann, A., Ditas, F., Seifert, P., Stratmann, F., Wiedensohler, A., Apituley, A., Shaw, R. A., Manninen, H. E., and Kulmala, M.: Observations of turbulence-induced new particle formation in the residual layer, *Atmos. Chem. Phys.*, 10, 4319–4330, <https://doi.org/10.5194/acp-10-4319-2010>, 2010.
- World Health Organization: Ambient air pollution: A global assessment of exposure and burden of disease, Tech. Rep., available at: <http://apps.who.int/iris/bitstream/10665/250141/1/9789241511353-eng.pdf?ua=1> (last access: 29 November 2018), 2016.
- Zhang, H., Surratt, J. D., Lin, Y. H., Bapat, J., and Kamens, R. M.: Effect of relative humidity on SOA formation from isoprene/NO photooxidation: enhancement of 2-methylglyceric acid and its corresponding oligoesters under dry conditions, *Atmos. Chem. Phys.*, 11, 6411–6424, <https://doi.org/10.5194/acp-11-6411-2011>, 2011.
- Zhang, Q., Worsnop, D. R., Canagaratna, M. R., and Jimenez, J. L.: Hydrocarbon-like and oxygenated organic aerosols in Pittsburgh: insights into sources and processes of organic aerosols, *Atmos. Chem. Phys.*, 5, 3289–3311, <https://doi.org/10.5194/acp-5-3289-2005>, 2005.
- Zhang, Q., Jimenez, J. L., Canagaratna, M. R., Allan, J. D., Coe, H., Ulbrich, I., Alfarra, M. R., Takami, A., Middlebrook, A. M., Sun, Y. L., Dzepina, K., Dunlea, E., Docherty, K., Decarlo, P. F., Salcedo, D., Onasch, T., Jayne, J. T., Miyoshi, T., Shimono, A., Hatakeyama, S., Takegawa, N., Kondo, Y., Schneider, J., Drewnick, F., Borrmann, S., Weimer, S., Demerjian, K., Williams, P., Bower, K., Bahreini, R., Cottrell, L., Griffin, R. J., Rautiainen, J., Sun, J. Y., Zhang, Y. M., and Worsnop, D. R.: Ubiquity and dominance of oxygenated species in organic aerosols in anthropogenically-influenced Northern Hemisphere midlatitudes, *Geophys. Res. Lett.*, 34, L13801, <https://doi.org/10.1029/2007GL029979>, 2007.
- Zhou, S., Collier, S., Xu, J., Mei, F., Wang, J., Lee, Y. N., Sedlacek, A. J., Springston, S. R., Sun, Y., and Zhang, Q.: Influences of upwind emission sources and atmospheric processing on aerosol chemistry and properties at a rural location in the Northeastern US, *J. Geophys. Res.-Atmos.*, 121, 6049–6065, 2016.

Supplement of Atmos. Chem. Phys., 19, 11123–11142, 2019
<https://doi.org/10.5194/acp-19-11123-2019-supplement>
© Author(s) 2019. This work is distributed under
the Creative Commons Attribution 4.0 License.



Supplement of

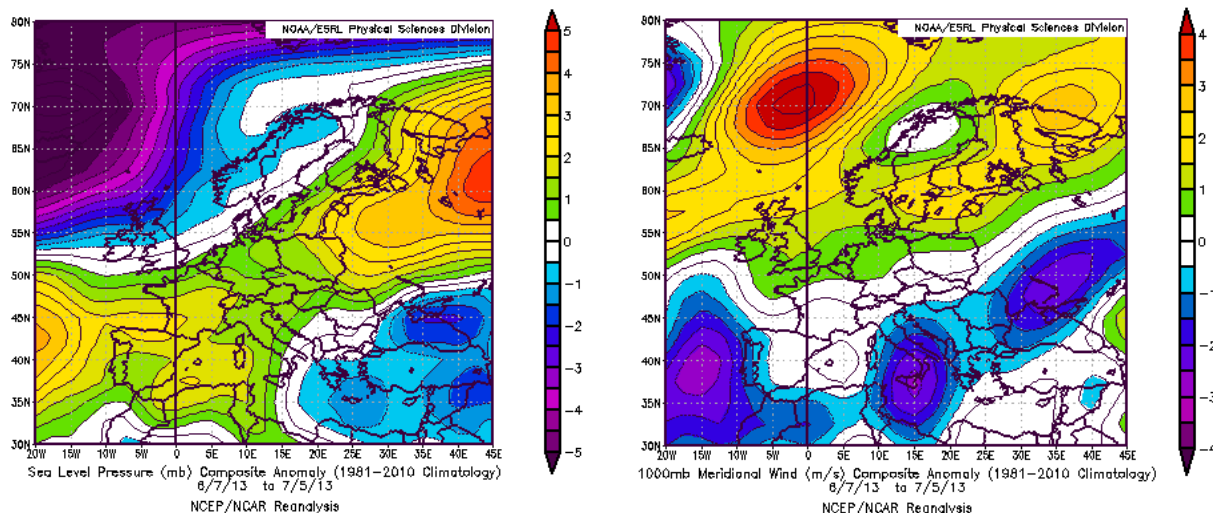
Summertime surface PM_{10} aerosol composition and size by source region at the Lampedusa island in the central Mediterranean Sea

Marc D. Mallet et al.

Correspondence to: Paola Formenti (paola.formenti@lisa.u-pec.fr)

The copyright of individual parts of the supplement might differ from the CC BY 4.0 License.

Synoptic scale meteorology



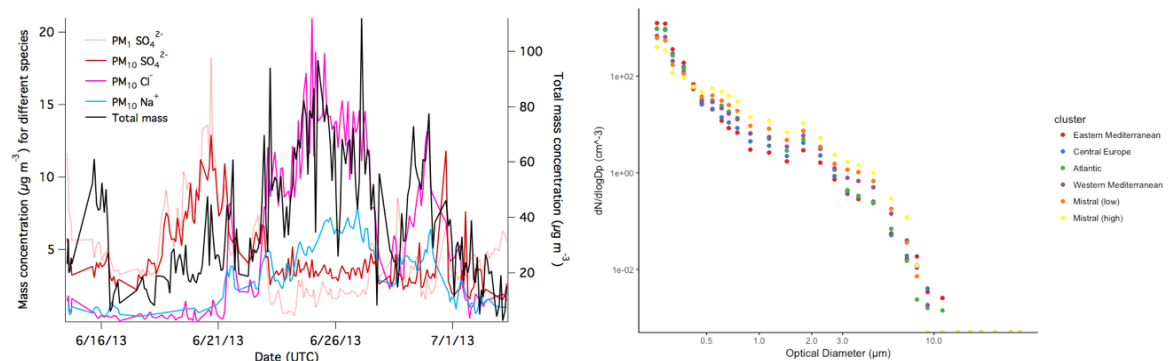
Supplementary Figure S1 Sea level pressure (left) and 1000 mb meridional wind component (right) composite anomalies of the ADRIMED campaign period with respect to the 1981-2010 climatology obtained from the NCEP/NCAR Reanalysis. Images were provided by the NOAA/ESRL Physical Sciences Division, Boulder Colorado (<http://www.esrl.noaa.gov/psd/>).

Origin of Sulphates

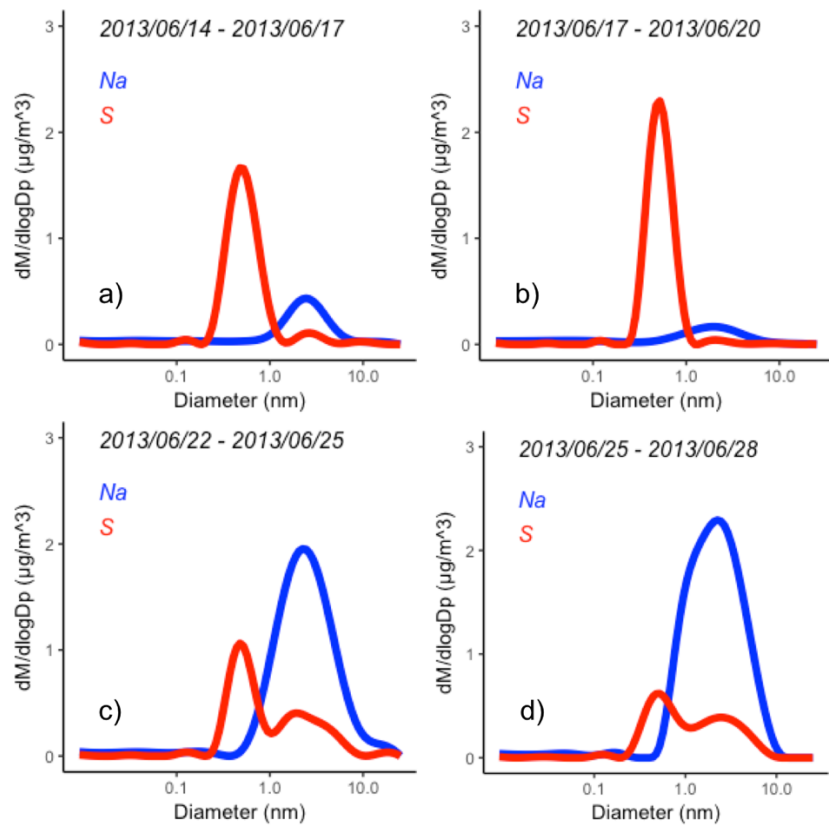
The total averaged aerosol mass concentration (PM_{total}) measured by the FDMS-TEOM during the campaign was $37 \mu\text{g m}^{-3}$ (maximum value up to $126 \mu\text{g m}^{-3}$). The PM_{total} was relatively well correlated with TSP concentrations of ions associated with sea salt (Na^+ , Mg^+ , Cl^-) measured by the PILS ($R^2 \sim 0.5$, not shown). The total TSP sea salt concentration, was less than half of the PM_{total} , suggesting that a significant fraction of coarse particles was not sea salt or soluble species. There was a positive correlation ($R^2=0.80$) throughout the measurement period between the Na^+ and Cl^- mass concentrations and wind speed (measured at the Lampedusa site) which is indicative of sea spray aerosol. Other trace elements associated with dust were low in concentration over the entire measurement period. As shown in Section 3.2, the highest observed sea salt concentrations throughout the campaign were observed during the "Mistral" air mass origin periods. These periods were accompanied by the highest wind speeds, likely a result of the rapid descent of the air masses after passing over southern France. Despite a relatively small accumulation mode, these Mistral air masses had the highest number of coarse mode particles which is consistent with the high sea salt concentrations.

For most of the campaign, there was good correlation between the PM_{10} and $TSP\ SO_4^{2-}$ concentrations, with the exception of periods of high sea salt concentrations. The 3-day samples obtained by the multistage cascade impactor show that majority of the elemental sulphur mass was within the PM_{10} size range.

However, during periods of high concentrations of sea salt, up to 48% of the elemental sulphur mass was associated with particles larger than $1\ \mu m$. Some of this can be explained by the presence of seasalt-S, although up to 40% of the total nss-S was still associated with coarse mode particles. The two samples in the period 14-17 June and from the 17-20 June, characterized mostly by central European and eastern Mediterranean air masses, show relatively low sea salt ion concentrations. For those, the non-sea-salt fraction of elemental sulphur (nss-S) was nearly all under $1\ \mu m$. During the periods of higher sea salt concentrations, there was a more pronounced partitioning of the nss-S between sub- and super-micron particles.

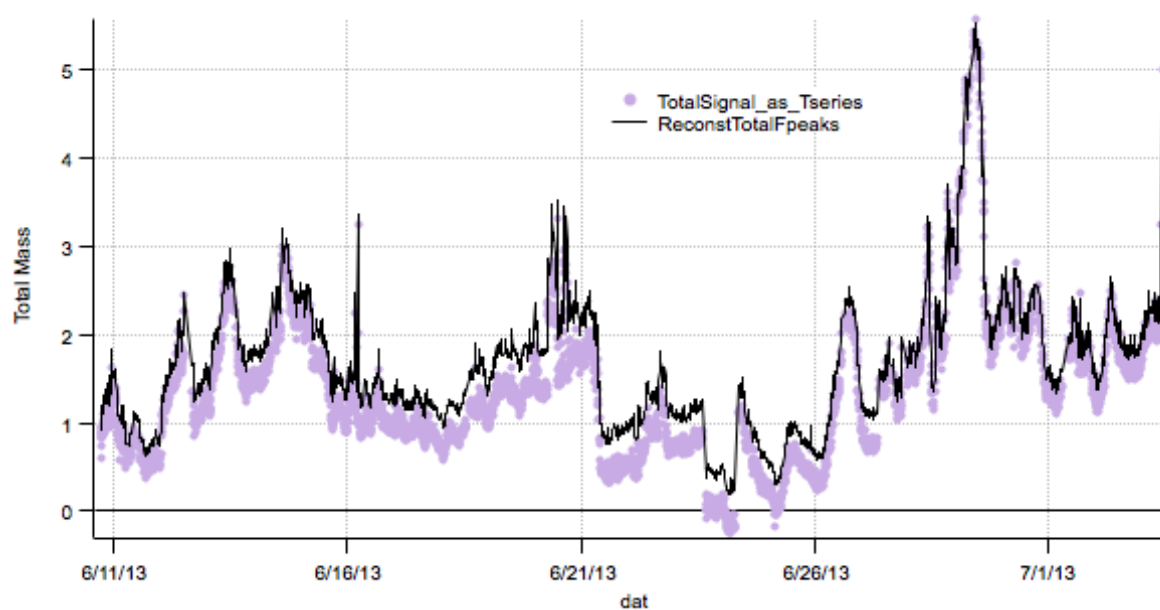


Supplementary Figure S2 (left) the time series of $TSP\ Cl^-$ and Na^+ , PM_{10} and $PM_{10}\ SO_4^{2-}$ and the total particle mass from the TEOM and (right) the size distribution above $0.26\ \mu m$, measured by the GRIMM OPC, with colours representing averages for different air mass origins.

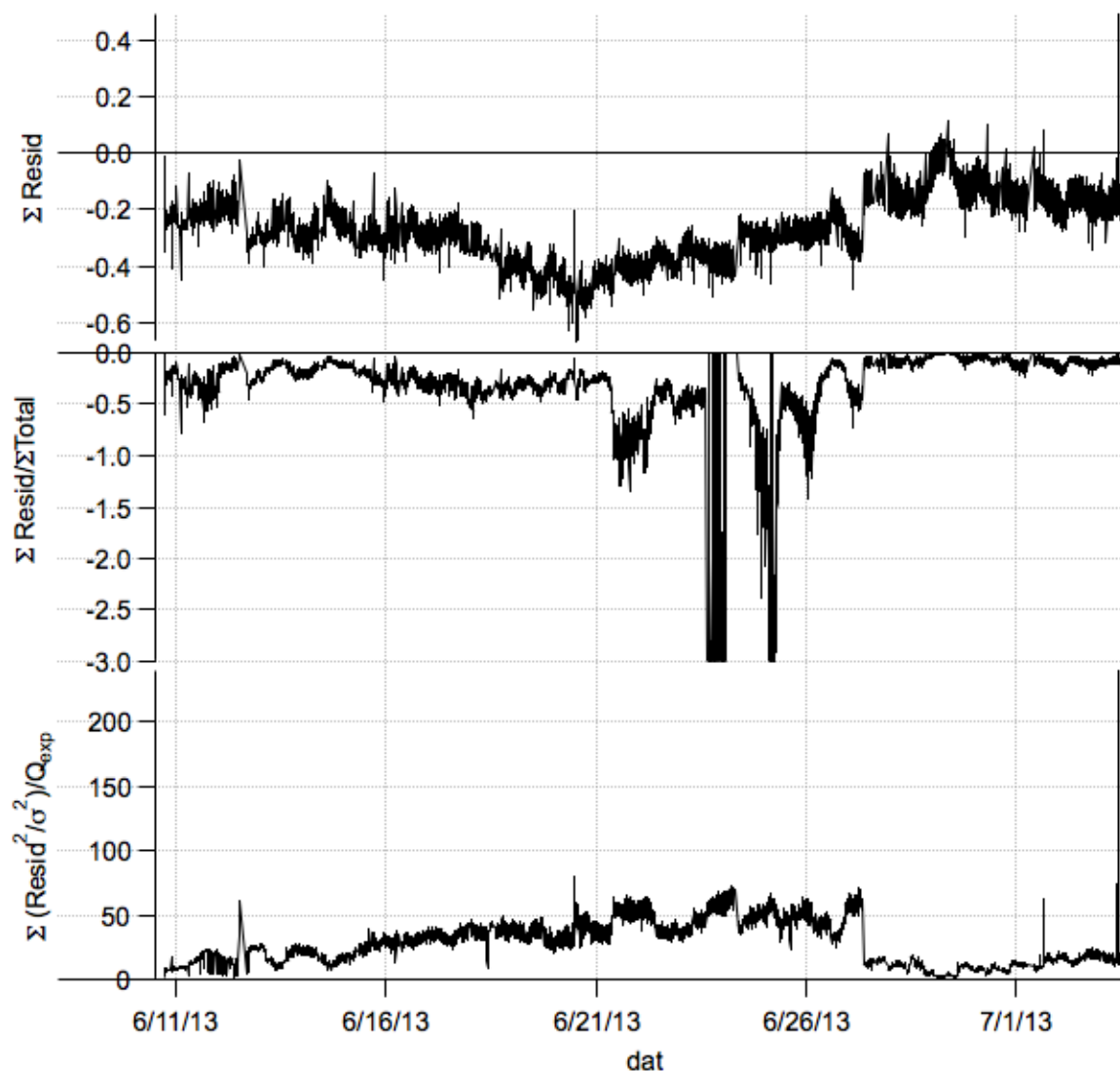


Supplementary Figure S3 Interpolated mass size distribution of Na^+ , Cl^- and nss-S for four different 3-day sampling periods, collected on a 13-stage cascade impactor. Note that the vertical scales are different in each graph.

PMF mass reconstruction and residuals



Supplementary Figure S4 Total organic signal and reconstructed from 4-factor PMF solution



Supplementary Figure S5 Time series of residuals from 4-factor PMF solution

Supplementary compositional material

Supplementary Table S1 A summary of studies that have investigated NR-PM₁ composition (including PMF of OA) at coastal sites surrounding the Mediterranean basin and in the remote Mediterranean. Only studies that have investigated PMF-based OA source apportionment are reported. MO-OOA: More oxidised oxygenated organic aerosol, LO-OOA: less oxidised oxygenated organic aerosol, HOA: Hydrocarbon-like Organic Aerosol, SV-OOA: Semi-volatile oxygenated Organic Aerosol, LV-OOA: Low-volatility oxygenated Organic Aerosol, BBOA: Biomass burning Organic Aerosol, COA: Cooking Organic Aerosol, OOA: Oxygenated Organic Aerosol, F4: "Factor -4" (unidentified PMF factor), IndOA: Industry-related Organic Aerosol, OB-OA: "Olive-branch Organic Aerosol. PMF factors in bold indicate secondary organic aerosol.

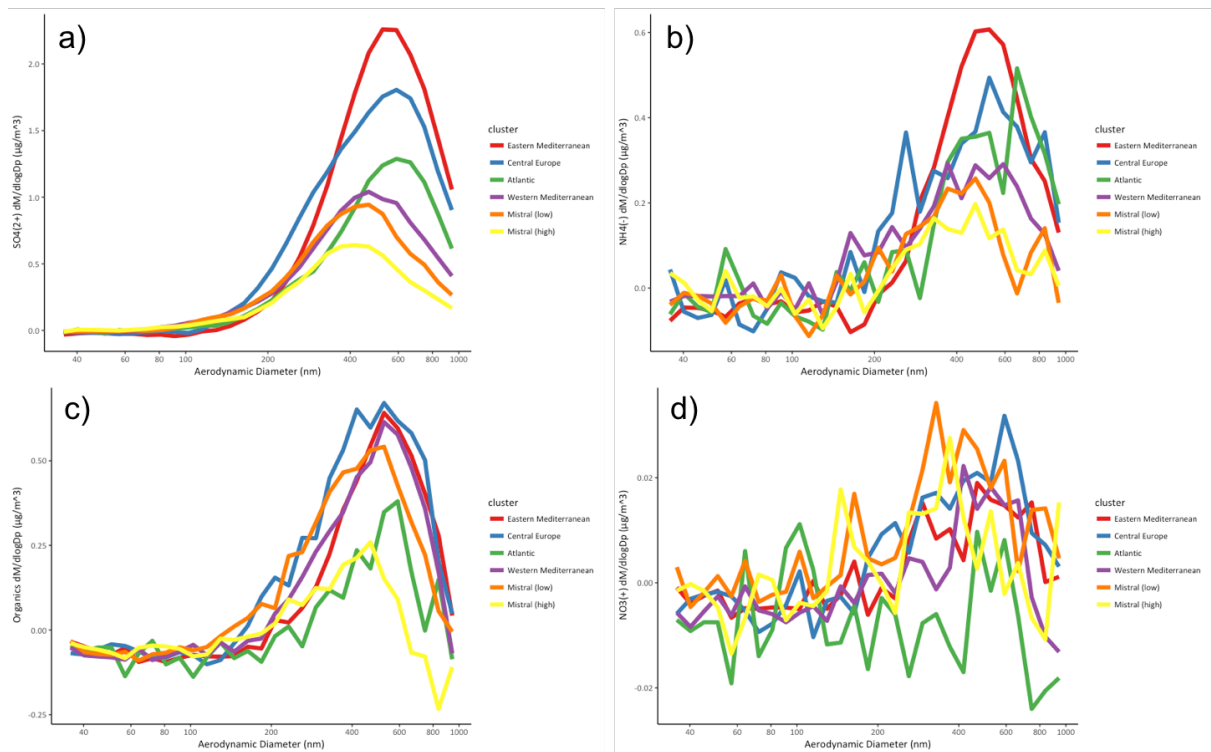
AUTHORS (YEAR)	LOCATION	PERIOD	INSTRUMENT	PM ₁ MASS COMPOSITION	AND	PMF FACTORS
THIS STUDY	Lampedusa	10 June - 5 July	cToF-AMS	10.1 μg m ⁻³ (OA: 30%, HOA (8%)		

	(35°31'5"N, 12°37'51"E, 45 m a.s.l.)	2013 (summer)		SO ₄ ²⁻ : 44%, NH ₄ ⁺ : 18%, NO ₃ ⁻ : 1%, seasalt: 1%, eBC: 5%)	MSA-OOA (12%) LO-OOA (28%) MO-OOA (53%)
(MINGUILLÓN ET AL., 2015)	Montseny (41°46'46"N, 02°21'19"E, 720 m a.s.l.)	June 2012 - July 2013	ACSM	Summer: 10.8 µg m ⁻³ (OA: 61%, SO ₄ ²⁻ : 21%, NH ₄ ⁺ : 9%, NO ₃ ⁻ : 4%, chloride: 1%, BC: 5%) Winter: 6.3 µg m ⁻³ (OA: 43%, SO ₄ ²⁻ : 8%, NH ₄ ⁺ + NO ₃ ⁻ +chloride: 49%)	Summer: HOA (13%) SV-OOA (41%) LV-OOA (44%) Winter: HOA (12%) BBOA (28%) OOA (59%)
(ARNDT ET AL., 2017)	Cape Corse (42°58'8.4"N, 9°22'48"E, 544 m a.s.l.)	11 June - 6 August 2013 (Summer)	Q-ACSM	5.5 µg m ⁻³ (OA: 55%, SO ₄ ²⁻ : 26, NH ₄ ⁺ : 13%, NO ₃ ⁻ : 5%)	SV-OOA (62%) LV-OOA (33%)
(MICHOUDET AL., 2017)	Cape Corse (42°58'8.4"N, 9°22'48"E, 544 m a.s.l.)	July 15 - August 5 2013 (Summer)	Q-ACSM	6.8 µg m ⁻³ (OA: 55%, SO ₄ ²⁻ : 27%, NH ₄ ⁺ : 13%, NO ₃ ⁻ : 5%)	HOA (4%) SV-OOA (44%) LV-OOA(53%)
(RINALDI ET AL., 2017)	Cape Granitola (37°34'31.1"N, 12°39'34.2"E, 5 m a.s.l.)	April 2016 (Spring)	HR-ToF-AMS	3.5 µg m ⁻³ (OA: 37%, SO ₄ ²⁻ : 31%, NH ₄ ⁺ : 12%, NO ₃ ⁻ : 3%, seasalt: 10%, BC: 6%)	HOA (3%) BBOA (2%) OOA-1 + OOA-2 (70%) OOA-3 (25%)
HILDEBREANDT ET AL., 2010	Finokalia (35°20'N, 25°40'E, 150 m a.s.l.)	May 2008 (Spring)	Q-AMS	9 µg m ⁻³ (OA: 28%, SO ₄ ²⁻ : 55%, NH ₄ ⁺ : 16%, NO ₃ ⁻ : 2%)	OOA-1 (61%) OOA-2 (39%)
HILDEBRANDT ET AL., 2011	Finokalia (35°20'N, 25°40'E, 150 m a.s.l.)	25 February - 26 March 2009 (late Winter)	Q-AMS	3.3 µg m ⁻³ (OA: 43%, SO ₄ ²⁻ : 42%, NH ₄ ⁺ : 14%, NO ₃ ⁻ : 2%)	OOA (>56%) OB-OA (15 - 35%) Amine-OA (6 - 21%)
BOUGIATIOTI ET AL., 2014	Finokalia (35°20'N, 25°40'E, 150 m a.s.l.)	August - September 2012	Q-ACSM	Fire events: OA: 46.5% , SO ₄ ²⁻ : 29.2%, NH ₄ ⁺ : 11.7%, NO ₃ ⁻ : 3.2%, BC: 9.5% Nonfire periods: OA: 34.7% , SO ₄ ²⁻ : 43%, NH ₄ ⁺ : 13.7%, NO ₃ ⁻ : 2.2%, BC: 6.1%	BBOA (<20%) OOA1-BB + OOA2 (>80%)
(MOHR ET AL., 2012)	Barcelona (41°23'24"N, 02°6'58.1"E, 80 m a.s.l.)	March (Spring)	2009 HR-ToF-AMS	18.5 µg m ⁻³ (OA: 43%, SO ₄ ²⁻ : 16%, NH ₄ ⁺ : 9%, NO ₃ ⁻ : 18%, BC: 12%, Chl: 1%)	HOA (16%) BBOA (11%) COA (17%) SV-OOA (27%) LV-OOA (28%)
(MINGUILLÓN ET AL., 2016)	Barcelona (41°23'14"N, 02°06'56"E, 78 m a.s.l.)	16 August - 6 September 2013	ACSM	10 - 14 µg m ⁻³ (OA: 59 - 57%, SO ₄ ²⁻ : 20%, NH ₄ ⁺ : 9 - 10%, NO ₃ ⁻ : 4 - 5%, EC: 8%)	COA (17%) HOA (8 - 10%) SV-OOA (38 - 40%) LV-OOA (36%)

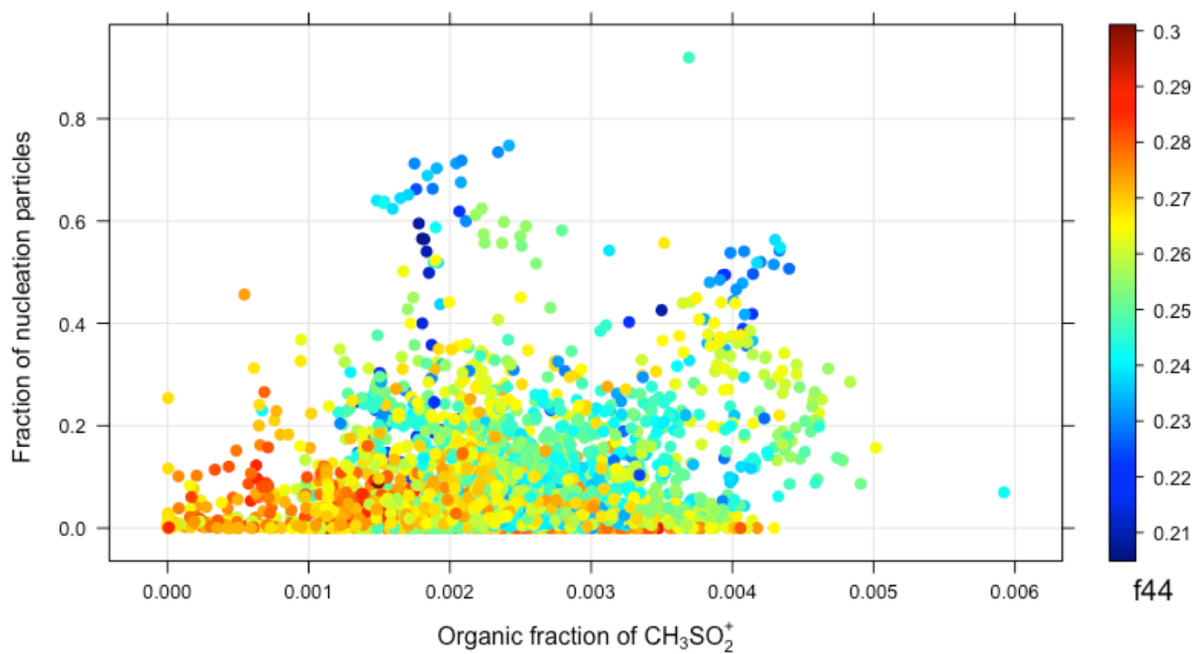
EL HADDAD ET AL., 2013	Marseille (43°18'20"N, 5°23'40"E, 64 m a.s.l.)	30 June - 14 July 2008 (Summer)	cToF-AMS	PM ₁ concentrations not explicitly stated. SO ₄ ²⁻ concentrations where generally similar or higher than OA.	HOA (19%) F4 (6%) SV-OOA (34%) LV-OOA (41%)
(BOZZETTI ET AL., 2017)	Marseille (43°18'20"N, 5°23'40"E, 64 m a.s.l.)	August 2011 - July 2012	HR-ToF-AMS (nebulized PM2.5 filters)	10 - > 50 µg m ⁻³ (OA: 37% - 51%, SO ₄ ²⁻ : 12%, NH ₄ ⁺ : 8%, NO ₃ ⁻ : 9%, EC: 9%, Other: 9%)	Summer: HOA (17%) BBOA (5%) COA (4%) OOA (55%) IndOA (11%) Winter: BBOA (48%) COA (4%) OOA (27%) IndOA (17%)

Supplementary Table S2 The average speciated PM₁ concentrations during periods of different air mass origin. Units are µg m⁻³.

Sector	Organics	SO ₄ ²⁻	NH ₄ ⁺	NO ₃ ⁻	Seasalt	eBC
Atlantic ocean	2.8±0.9 (MO-OOA: 55%, LO-OOA: 24%, MSA-OOA: 11%, HOA: 9%)	4.0±1. 5	1.7±0. 6	0.91±0.0 3	0.25±0.09	0.46±0.0 8
Western Europe	3.0±1.3 (MO-OOA: 44%, LO-OOA: 38%, MSA-OOA: 10%, HOA: 8%)	3.5±1. 6	1.4±0. 6	0.10±0.0 5	0.35±0.18	0.51±0.0 9
Mistral (high)	1.7±0.4 (MO-OOA: 37%, LO-OOA: 36%, MSA-OOA: 23%, HOA: 4%)	2.0±0. 5	0.9±0. 2	0.06±0.0 2	0.29±0.04	0.36±0.1 4
Mistral (Low)	3.2±1.1 (MO-OOA: 41%, LO-OOA: 40%, MSA-OOA: 12%, HOA: 7%)	2.9±1. 4	1.3±0. 5	0.11±0.0 6	0.41±0.17	0.50±0.1 0
Central Europe	3.8±0.8 (MO-OOA: 58%, LO-OOA: 23%, MSA-OOA: 11%, HOA: 8%)	6.4±1. 8	2.4±0. 5	0.13±0.0 5	0.26±0.07	0.53±0.1 7
Eastern Med.	3.1±0.6 (MO-OOA: 71%, LO-OOA: 14%, MSA-OOA: 6%, HOA: 8%)	6.7±3. 1	2.8±1. 3	0.09±0.0 3	0.19±0.06	0.55±0.1 2
Campaign average	3.0±1.1 (MO-OOA: 53%, LO-OOA: 28%, MSA-OOA: 12%, HOA: 8%)	4.5±2. 7	1.9±1. 0	0.10±0.0 5	0.30±0.15	0.50±0.2 1



Supplementary Figure S6 The average size distribution of sulphates, ammonium, organics and nitrates, measured by the cToF-AMS with colours representing the different air mass origins.



Supplementary Figure S7 The fraction of nucleation particles (particle number concentration between 14 and 25 nm divided by the particle number concentration between 14 and 600 nm), as a function of the organic fraction of $PM_{10}CH_3SO_2^+$